This paper is available on line at http://www.mcponline.org

Integrated Transcriptional and Proteomic Analysis with *In Vitro* Biochemical Assay Reveal the Important Role of CYP3A46 in T-2 Toxin Hydroxylation in Porcine Primary Hepatocytes*[S]

Jianshe Wang‡‡‡, Jun Jiang§‡‡, Hongxia Zhang‡, Junping Wang§, Hua Cai§, Cheng Li¶, Kangbai Li§, Jing Liu§, Xuejiang Guo¶, Guangxun Zou‡, Dazhi Wang‖, Yiqun Deng§, and Jiayin Dai‡¶****

Both T-2 toxin and its metabolites are highly potent mycotoxins that can cause severe human and animal diseases upon exposure. Understanding the toxic mechanism and biotransformation process of T-2 toxin at a cellular level is essential for the development of countermeasures. We investigated the effect of T-2 toxin in porcine primary hepatocytes using porcine genome array and two-dimensional difference gel electrophoresis with matrix-assisted laser desorption/ionization tandem time of flight mass spectrometry. Integrated transcriptional and proteomic analysis demonstrated that T-2 toxin adversely affected porcine hepatocytes by initiating lipid metabolism disorder, oxidative stress response, and apoptosis. In addition, xenobiotic metabolism genes, including cytochrome P450 3As (CYP3A46 and CYP3A39), carboxylesterase 1Cs (CES1C4 and CES1C5), and epoxide hydrolase (EPHX1), increased in T-2 toxin treatment cells. Using HepG2 cells to over-express the recombinant xenobiotic metabolism genes above and rapid resolution liquid chromatography/tandem mass spectrometry to detect metabolites of T-2 toxin, we determined that porcine CYP3A46 mainly catalyzed T-2 to form 3′-hydroxy-T-2, which was further confirmed by purified CYP3A46 protein. However, recombinant porcine CES1C5 and EPHX1 did not enhance hydrolysis and de-epoxidation of T-2 implying that other esterases and epoxide hydrolases may play dominant roles in those reactions. ***Molecular & Cellular Proteomics 10: 10.1074/mcp.M111.008748, 1–18, 2011.***

From the ‡Key Laboratory of Animal Ecology and Conservation Biology, Institute of Zoology, Chinese Academy of Sciences, Beijing, 100101, China; §College of Life Sciences, South China Agricultural University, Guangzhou, 510642, China; ¶State Key Laboratory of Reproductive Medicine, Department of Histology and Embryology, Nanjing Medical University, Nanjing 210029, China; ‖State Key Laboratory of Marine Environmental Science/Environmental Science Research Center, Xiamen University, Xiamen 361005, China

Received February 13, 2011, and in revised form, June 15, 2011

Published, MCP Papers in Press, June 16, 2011, DOI 10.1074/mcp.M111.008748

The T-2 toxin is a sesquiterpenoid fungal metabolite belonging to A-trichothecenes. It is a highly toxic mycotoxin produced by different *Fusarium* species, which can infect crops during growth and storage (1, 2). Type A-trichothecenes have a characteristic 12,13-epoxytrichothecene-9-ene ring structure, which specifically relates to its toxicity (3, 4). These substances have been detected in food samples around the world (5–7) and consumption can instigate toxic reactions such as prostration, weakness, ataxia, collapse, reduced cardiac output, and at extremely high doses, shock-like syndrome and death (8). Chronic exposure to trichothecenes can cause anorexia, reduced weight gain, diminished nutritional efficiency, neuroendocrine changes, bone marrow aplasia, and immune modulation (9, 10). Reports have shown that increased levels of T-2 and its HT-2 toxin (HT-2) metabolite have been detected in food samples beyond tolerable daily levels in several countries (11).

A variety of mechanisms have been proposed for how T-2 works (12) including reaction with thiol groups of sulfhydryl enzymes that inhibit protein and DNA synthesis (13), as well as increased levels of reactive oxygen species (ROS)[1], which impair antibody production (14), alter membrane function (15), reduce lymphocyte proliferation (16), and cause apoptosis (17).

After absorption, T-2 rapidly converts into its metabolites. Several biotransformation reactions (such as hydrolysis, hydroxylation, de-epoxidation, and conjugation) occur during T-2 metabolism and numerous metabolites have been iden-

[1] The abbreviations used are: CES, carboxylesterase; CYP, cytochrome P450; 2-D DIGE, two-dimensional difference gel electrophoresis; EPHX, epoxide hydrolase; RRLC/MS/MS, rapid resolution liquid chromatography/tandem mass spectrometry; MALDI-TOF MS/MS, matrix-assisted laser desorption ionization time-of-flight tandem mass spectrometry; DOPC, 1, 2-Dioleoyl-sn-glycero-3-phosphocholine; DLPC, 1, 2-Didodecanoyl-rac-glycero-3-phosphocholine; PS, 1, 2-Diacyl-sn-glycero-3-phospho-L-serine.

tified (5, 18). In swine, for example, more than 20 metabolites have been identified in tissues and the gastrointestinal tract (19), and the toxicity of T-2 may be attributed partly to these biotransformed products. Though the spectrum and amount of metabolites in animals strongly depends on the investigated species (5), the main biotransformation pathway that has been detected is deacetylation of the C-4 acetyl group of T-2 to HT-2 (18, 20, 21). Previous research has shown, however, that the cleavage of the acetyl group at position C-4 does not significantly affect toxicity. After the transformation of T-2 to HT-2, HT-2 undergoes further hydroxylation at C-3′ to yield 3′-hydroxy-HT-2. It also undergoes a hydroxylation reaction, especially at C-3′, to produce 3′-hydroxy-T-2. Except for HT-2, 3′-hydroxy-HT-2, and 3′-hydroxy-T-2, which are major metabolites, T-2 triol, T-2 tetraol, and deepoxy metabolites including deepoxy-HT-2, deepoxy-T-2 triol, and deepoxy-T-2 tetraol are also found in swine (22). Cytochrome P450 (CYP), esterase, and epoxide hydrolase (EPHX) are involved in the hydroxylation, hydrolysis, and de-epoxidation reactions of T-2, respectively. However, the exact CYP, esterase and EPHX isoforms responsible for T-2 biotransformation remain unclear (23).

Porcine hepatocytes in primary culture were chosen as the experimental model because of the high similarity of porcine and human liver drug metabolizing enzymes (24). Porcine hepatocytes are at greater risk of T-2 exposure, as much swine feed is comprised of cereal grain. Furthermore, T-2 has the potential to enter the human body from animals fed with contaminated feed. Understanding the molecular mechanism of T-2 toxicity, its biotransformation processes, and the enzymes involved in these processes is essential to predict potential deleterious effects and develop counter-measures. Recent innovations in genomic and proteomic technologies may help clarify the complex toxic mechanisms of T-2. Both cDNA microarray and proteomic analysis have been used to analyze gene expression and identify protein markers for many toxic chemicals (25–27). Here we simultaneously used porcine microarray and two-dimensional differential in-gel electrophoresis (2-D DIGE) with matrix-assisted laser desorption ionization time-of-flight tandem mass spectrometry (MALDI-TOF MS/MS) to determine the cytotoxic effects of T-2 and investigate candidate enzymes responsible for the metabolic transformation of T-2. We further confirmed these enzymes by *in vitro* biochemical assay.

EXPERIMENTAL PROCEDURES

Chemicals and Reagents—We purchased T-2, HT-2, nifedipine, oxidized nifedipine, ketoconazole, and NADPH from Sigma-Aldrich. Dulbecco's modified eagle's medium (DMEM) and fetal bovine serum (FBS) were obtained from Invitrogen (Carlsbad, CA). Acetonitrile (ACN) and water used in liquid chromatography (LC)-tandem mass spectrometry were obtained from Fisher Scientific and Milli-Q ultrapurification system (Millipore, Bedford, MA), respectively. All other chemicals including CHAPS, dithiothreitol (DTT), and phenylmethylsulfonyl fluoride (PMSF) were obtained from GE Healthcare (Uppsala, Sweden) or Merck (Darmstadt, Germany) unless otherwise mentioned.

Porcine Hepatocyte Isolation, Culture, and T-2 Treatment—All experimental procedures were approved by the Institute of Animal Care and Use Committee of the Institute of Zoology, Chinese Academy of Sciences, and were within the guidelines for use of laboratory animals. Animals (3-day-old domestic Chinese piglets crossbred from the Duroc, Large Yorkshire, and Landrace breeds) were euthanized using electric stunning followed by exsanguination. Hepatocytes were isolated by modified two-step *in situ* collagenase perfusion (details in supplemental Data) (28). They were then cultured in William's E medium (Sigma-Aldrich) containing 5% FBS, 100 U/ml of penicillin/streptomycin, 10^{-6} mM of insulin, and 10^{-6} mM of dexamethasone (Sigma-Aldrich).

For treatment, T-2 dissolved in dimethyl sulfoxide (Sigma-Aldrich) was added to the medium in concentrations of 0.02, 0.05, and 0.1 μg/ml, which were then incubated for 48 h. Control cells were incubated with an equal solvent concentration. The 0.05 μg/ml T-2 dose was selected for microarray and 2-D DIGE analysis based on our previous 3-(4,5-dimethylthiazol-2-yl)-2,5-diphenyltetrazolium assay (29).

RNA Isolation and cRNA Preparation—After T-2 treatment, total RNA was isolated from the porcine hepatocytes using Trizol Reagent (Invitrogen, Carlsbad, CA) according to manufacturer's protocols. After DNase I treatment, the RNA was cleaned up with a RNeasy Kit (Qiagen, Hilden, Germany), then quantitated spectrophotometrically. Integrity was checked by running 1 μg of RNA on a 1% agarose gel. The RNA was stored at −80 °C until processing. Six samples, three from the control group and three from the 0.05 μg/ml T-2 treatment group, were selected for microarray analysis. The RNA samples were processed according to manufacturer's instructions (details in supplemental Data) (Affymetrix, 701021 Rev.5, CA, USA).

Microarray Hybridization, Pathway Analysis, and Real-time PCR—Fragmented cRNA was individually hybridized with the GeneChip Porcine Genome Array (Affymetrix, Santa Clara, CA), which contained 23,937 probes (23,256 transcripts) representing 20,201 *Sus scrofa* genes. Hybridization, data capture, and analysis were performed by CapitalBio Corp (CapitalBio, Beijing, China). Briefly, a hybridization mixture was prepared for each sample containing 15 μg of fragmented cRNA, control oligo B2, and eukaryotic hybridization controls (bioB, bioC, bioD, cre), hybridization mix, and dimethyl sulfoxide. Sample mixtures (three controls and three treatments) were loaded onto six arrays and incubated at 45 °C for 16 h according to manufacturer's instructions. The probe arrays were washed and stained with streptavidin phycoerythrin using the Fluidics Station 450 (Affymetrix, Santa Clara, CA). Arrays were scanned immediately after washing and staining using the GeneChip Scanner 3000 7G (Affymetrix). Quantitative analysis of microarray hybridization was performed using Affymetrix MicroArray Suite 5.0-Specific Terms (Statistical Algorithms) GCOS (Affymetrix GeneChip Operating Software) Version 1.4.

Quantitative real-time PCR was performed to validate the microarray analysis results, and to determine the expression levels of selected genes from the 0.02 and 0.1 μg/ml T-2 exposed groups (details in the supplemental Data). Fold differences in expression levels were calculated using the $2^{-\Delta\Delta Ct}$ method (30). Primers and the amplicon sizes are listed in supplemental Table S1.

2-D DIGE and MALDI TOF/TOF Analysis—The primary hepatocytes from the control and 0.05 μg/ml T-2 treatment groups were homogenized in 1 ml of lysis buffer (7 M of urea, 4% CHAPS, 30 mM of Tris, 1.0% DTT, and 1 mM of PMSF). The homogenates were centrifuged at 20,000 × *g* for 20 min at 4 °C. The 2-D Clean-Up Kit (GE Healthcare, Uppsala, Sweden) was used to remove ionic interfering components from the protein extraction. Protein quantification in the urea-containing protein samples was performed using a 2D Quant Kit (GE Health-

TABLE I

Altered transcripts associated with xenobiotic metabolism, lipid metabolism, stress response, and apoptosis (twofold change or greater, $p < 0.05$) in the porcine hepatocytes treated by 0.05 μg/ml T-2[st]

Gene name	Gene symbol	Genbank accession no.	Fold change	Q value
Lipid metabolic process[a]				
acyl-Coenzyme A dehydrogenase, long chain	ACADL	NM_213897	2.38[b]	0
fatty acid desaturase 1	FADS1	BG834110	−4.35	0
fatty acid desaturase 2	FADS2	CF791131	−2.78	0
fatty acid synthase	FASN	CN166778	−5.00	0
lipase, hepatic	LIPC	BX675010	2.05	0
low density lipoprotein receptor	LDLR	BX667248	−4.55	0
peroxisome proliferator activated receptor gamma, coactivator 1 alpha	PPARGC-1	AB106108	−2.17	0
peroxisome proliferator-activated receptor gamma	PPARG	AB097926	−3.85	0
stearoyl-CoA desaturase	SCD	NM_213781	−2.27	0
Phase I reaction				
carboxylesterase 1C4	CES1C4	NM_214246	4.57	0
cytochrome P450 3A39	CYP3A39	NM_214422	2.40	0
cytochrome P450 3A46	CYP3A46	AB052266	7.08	0
cytochrome P450 C42	CYP2C42	Z93098	2.33	0
cytochrome P450, family 51, subfamily A, polypeptide 1	CYP51	NM_214432	−4.35	0
epoxide hydrolase	EPHX1	NM_214355	4.65	0
vitamin D3 25-Hydroxylase	CYP2D25	NM_214394	−3.13	0
Apoptosis and stress response				
BCL2-associated X protein	BAX	AJ606301	4.49	0
caspase 1, apoptosis-related cysteine peptidase	CASP1	NM_214162	4.89	0
caspase-15	LOC641352	BI347127	2.82	0
90 kDa heat shock protein	HSP90AA1	NM_213973	3.32	0
glutathione peroxidase 1	GPX1	NM_214201	2.43	0

[a] The transcripts were grouped according to their functions.

[b] Positive values represent up-regulation after treatment; negative values represent down-regulation after treatment.

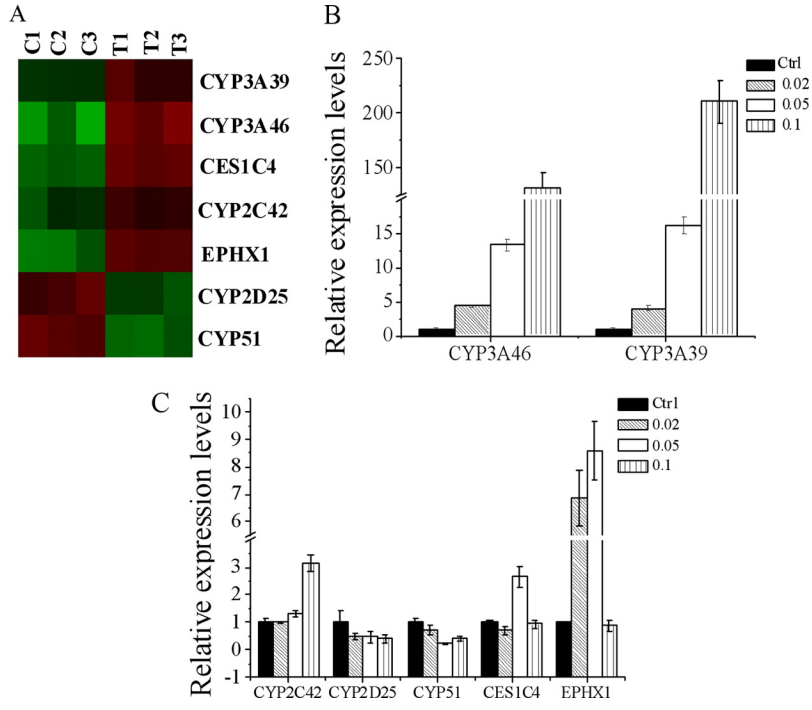

FIG. 1. **Differential mRNA levels of cytochrome P450s, CES1C4, and EPHX1 in T-2 toxin treatment porcine hepatocytes.** *A*, Heat map depicting expression levels of cytochrome P450s, CES1C4, and EPHX1 in porcine hepatocytes exposed to 0.05 μg/ml T-2 and control group. Each column displays the gene expression levels in individual samples and each row corresponds to the individual genes. *B*, *C*, Real-time PCR analysis of cytochrome P450s, CES1C4, and EPHX1 in 0.02, 0.05, and 0.1 μg/ml T-2 treatment porcine hepatocytes. Bars represent the relative fold changes compared with controls. Error bars represent the S.E. for the average fold changes. Statistical significance ($p < 0.05$ or $p < 0.01$) between expression after T-2 treatment and the controls is denoted by asterisks (* or **).

care). Samples were labeled by DIGE minimal labeling with Cy3 or Cy5 according to manufacturer's instructions (GE Healthcare, Uppsala, Sweden). The details of the 2-D DIGE and image analysis are described in the supplemental Data.

For picking protein spots of interest, the gels were fixed in 50% (v/v) ethanol and 10% (v/v) glacial acetic acid overnight, and then visualized by silver staining. The spots of interest were manually excised from the silver-stained gels and subjected to in-gel trypsin

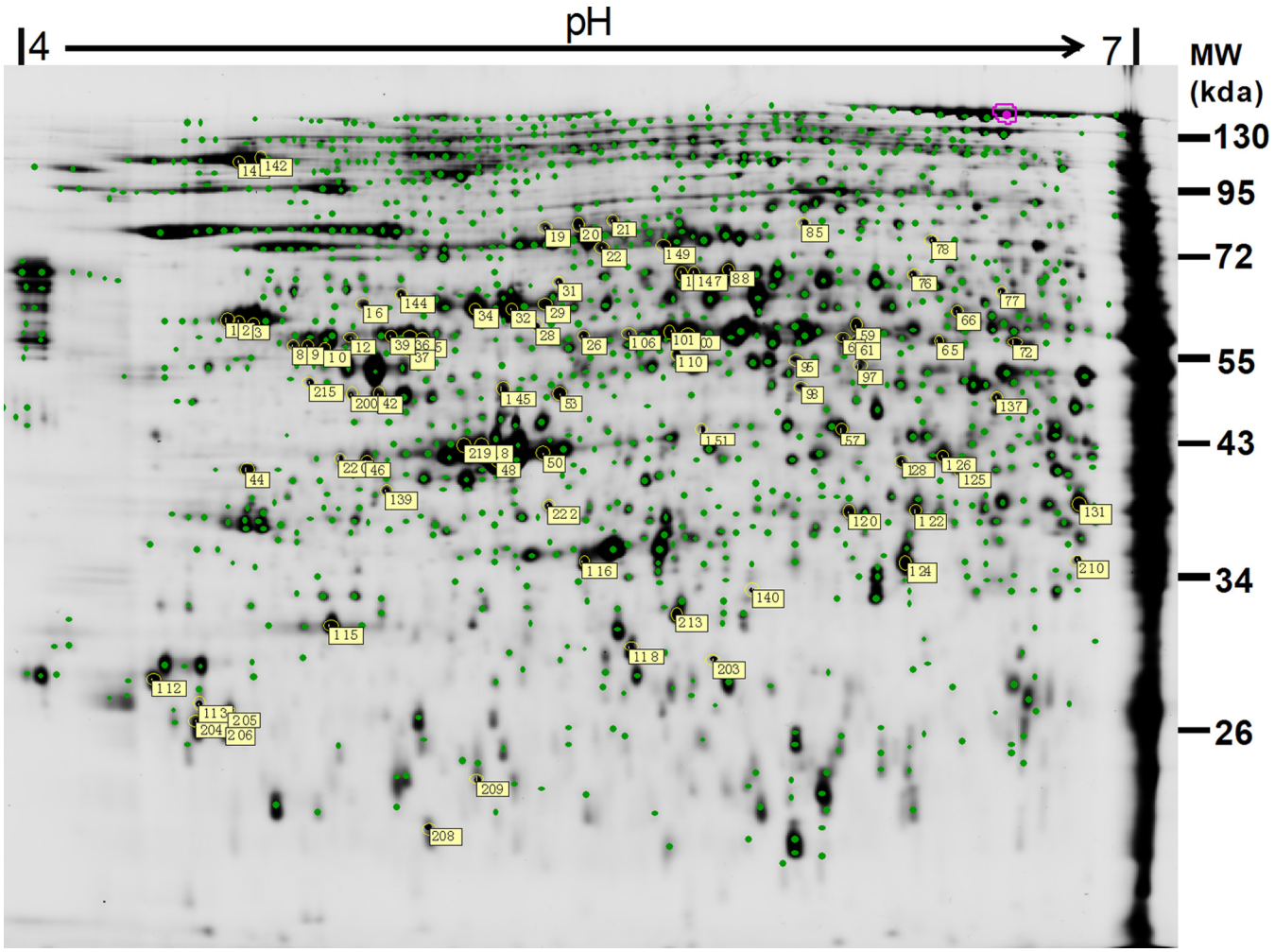

FIG. 2. **Representative image of two-dimensional DIGE showing location of differential protein spots identified by MALDI-TOF/TOF.** Porcine hepatocyte proteins in the control and 0.05 μg/ml T-2 treatment group were labeled with DIGE Fluor dye and separated on a linear IPG strip (pH 4–7) in the first dimension and on a 12.5% SDS-polyacrylamide gel in the second dimension. Protein spots altered by T-2 exposure and identified successfully by MALDI-TOF/TOF mass were labeled by numbers as listed in Table II.

digestion. After digestion, peptides were then extracted twice using 0.1% trifluoroacetic acid (TFA) in 50% ACN. The extracts were pooled and dried completely by SpeedVac. Peptide mixtures were redissolved in 0.1% trifluoroacetic acid , and 0.8 μl of peptide solution was mixed with 0.4 μl of matrix (α-cyano-4-hydroxycinnamic acid (CHCA) in 30% ACN, 0.1% trifluoroacetic acid) before spotting on the target plate.

Protein identification was performed on an AB SCIEX MALDI TOF-TOF™ 5800 Analyzer (AB SCIEX, Foster City, CA) equipped with a neodymium: yttrium-aluminum-garnet laser (laser wavelength was 349 nm). The TOF/TOF calibration mixtures (AB SCIEX) were used to calibrate the spectrum to a mass tolerance within 150 ppm. For MS mode, peptide mass maps were acquired in positive reflection mode, and 850–4000 *m/z* mass range was used with 1000 laser shots per spectrum. The PMF peak detection criteria used were a minimum signal-to-noise (S/N) of 10, local noise window width mass/charge (m/z) of 250, and minimum full-width half-maximum (bins) of 2.9. A maximum of 20 precursors per spot with a minimum signal/noise ratio of 50 were selected for MS/MS analysis using ambient air as the collision gas with medium pressure of 10^{-6} Torr. The contaminant *m/z* peaks originating from human keratin, trypsin auto-digestion, or matrix were excluded for MS/MS analysis. Energy of 1 KV was used for collision-induced dissociation, and 2000 acquisitions were accumulated for each MS/MS spectrum. The peak detection criteria used were a minimum S/N of 3, local noise window width (*m/z*) of 200, and minimum full-width half-maximum (bins) of 2.9. A combined MS and MS/MS search was performed against the NCBI nr database for other mammalian species (updated February, 2011, containing 382,684 entries) except primates and rodents. All automatic data analysis and database searching were conducted using GPS Explorer™ software (version 3.6, AB SCIEX) running a mascot search algorithm (v2.2, Matrix Science, London, UK) for protein identification.

The raw MS and MS/MS spectra were processed using GPS Explorer™ software with the following criteria: MS peak filtering-mass range, 850–4000 Da; minimum signal-to-noise ratio of 10; peak density filter of 50 peaks per 200 Da; maximum of 65 peaks; and MS/MS peak filtering-mass range of 60–20 Da below each precursor mass. The searches were conducted using the following settings: trypsin as digestion enzyme, one missed cleavage, 100 ppm precursor tolerance, MS/MS ion tolerance of 0.4 Da, carbamidomethylation of cysteine as fixed modification, and methionine oxidation as variable modification. The contaminant *m/z* peaks originating from human keratin, trypsin auto-digestion, or matrix were excluded. Proteins with protein score confidence intervals (C.I.) above 95% (protein score >

TABLE II

Detailed list of differentially expressed protein spots (1.2-fold change or greater, $p < 0.05$) identified by MALDI-TOF/TOF from the porcine hepatocytes following 0.05 μg/ml T-2 treatment (score C. I > 95%)

Spot no.[a]	Name	Species	Genbank identifier (gi)	Protein score	Total ion score[b]	Unique peptides detected	Sequence coverage (%)	Fold change[c]
Cytoskeleton[d]								
213	ANXA4	Sus scrofa	264681432	1300	1002	29	75	−2.13
22	PLS3	*Sus scrofa*	194044901	814	586	26	48	−1.52
115	ANXA5	*Bos taurus*	260137	623	459	18	57	−1.47
37	TUBA1B	*Mus musculus*	34740335	1030	761	26	63	−1.31
36	TUBA1B	*Mus musculus*	34740335	1300	1024	26	61	−1.37
10	1TUB_B	*Sus scrofa*	3745822	1240	972	25	68	−1.34
8	LOC100152382	*Sus scrofa*	194040124	697	480	23	50	−1.29
12	LOC100152382	*Sus scrofa*	194040124	490	302	21	49	−1.33
9	1TUB_B	*Sus scrofa*	3745822	915	685	23	66	−1.28
48	LOC414396	*Sus scrofa*	45269029	1180	949	23	57	−1.28
35	TUBA1A	*Sus scrofa*	194043861	1300	1057	24	50	−1.20
50	ACTB	*Sus scrofa*	45269029	1230	1017	22	63	−1.27
39	TUBA1A	*Sus scrofa*	194043861	926	719	22	53	−1.23
Protein binding								
46	KRT19	*Bos taurus*	62751472	380	254	17	37	−1.71
219	KRT18	*Sus scrofa*	157382506	281	210	9	35	−1.40
106	KRT8	*Sus scrofa*	227430407	682	469	27	50	−1.29
218	KRT18	*Sus scrofa*	157382506	291	220	9	38	−1.20
100	KRT8	*Sus scrofa*	227430407	1060	764	32	67	−1.22
101	KRT8	*Sus scrofa*	227430407	967	654	33	67	−1.30
220	KRT19	*Bos taurus*	62751472	358	232	17	34	−1.23
205	YWHAG	*Bos taurus*	71153781	641	509	15	47	−1.24
76	CORO1B	*Equus caballus*	194218536	522	353	21	32	−1.22
78	ALB	*Sus scrofa*	833798	501	308	25	37	1.33
Stress response								
149	HSPA1B	*Sus scrofa*	47523308	179	142	10	18	−1.20
208	PRDX2	*Sus scrofa*	1717797	605	537	7	45	−1.22
34	HSPD1	*Sus scrofa*	194044029	1530	1293	27	59	1.25
32	HSPD1	*Sus scrofa*	194044029	1300	1156	20	46	1.24
29	HSPD1	*Sus scrofa*	194044029	698	647	11	25	1.23
142	HSP90B1	*Sus scrofa*	17865698	878	644	32	36	1.34
141	HSP90B1	*Sus scrofa*	17865698	857	596	34	41	1.48
77	CAT	*Sus scrofa*	50979303	386	297	14	26	1.27
Electron transport								
128	NDUFA9	*Equus caballus*	149711435	523	437	12	35	1.28
53	UQCRC1	*Sus scrofa*	311268859	1270	1003	26	59	1.37
20	NDUFS1	*Canis lupus familiaris*	74005204	868	637	28	37	1.31
19	NDUFS1	*Canis lupus familiaris*	74005204	318	161	22	31	1.31
21	NDUFS1	*Canis lupus familiaris*	74005204	760	607	22	33	1.63
Lipid metabolism								
61	ALDH7A1	*Bos taurus*	187960116	251	218	8	17	1.27
126	ACADSB	*Sus scrofa*	194041602	369	269	14	35	−1.24
203	HSD17B8	*Sus scrofa*	195539468	594	521	9	46	1.20
72	ALDH7A1	*Bos taurus*	187960116	492	423	12	24	1.21
65	ALDH7A1	*Bos taurus*	187960116	407	358	10	19	1.21
66	PCCB	*Sus scrofa*	47522682	1080	874	24	55	1.22
125	ACADS	*Sus scrofa*	47522686	452	393	11	29	1.24
Signal transduction								
112	MSFL	*Canis lupus familiaris*	73967154	440	361	12	44	−1.34
204	YWHAZ	*Bos taurus*	192988247	581	453	15	55	−1.42
113	YHAWZ	*Canis lupus familiaris*	73974186	273	213	9	43	−1.29
206	KCIP-1	*Canis lupus familiaris*	73992052	384	288	11	47	−1.28
16	GDI1	*Canis lupus familiaris*	50978936	152	93	11	29	−1.22
Others								
118	PHB	*Equus caballus*	149723936	1200	956	22	89	1.24
146	CES1C4	*Sus scrofa*	47523572	696	524	21	41	1.30
88	CES1C5	*Sus scrofa*	2494384	1020	735	29	53	1.32
1	P4HB	*Bos taurus*	148878430	179	154	6	17	1.33
2	P4HB	*Bos taurus*	148878430	544	447	15	32	1.34
3	P4HB	*Bos taurus*	148878430	271	217	10	23	1.30
42	PDIA6	*Equus caballus*	149728149	627	528	14	36	1.38

TABLE II—*continued*

Spot no.[a]	Name	Species	Genbank identifier (gi)	Protein score	Total ion score[b]	Unique peptides detected	Sequence coverage (%)	Fold change[c]
200	TXNDC4	*Sus scrofa*	212549623	401	299	14	33	1.50
97	ENO1	*Rattus norvegicus*	59808815	284	205	12		−1.49
85	PGM2	*Bos taurus*	151554318	91	67	7	10	−1.48
60	GLYCTK	*Equus caballus*	149728822	196	163	8	10	1.24
28	HNRNPK	*Bos taurus*	77736071	401	326	13	24	−1.48
144	HNRNPK	*Bos taurus*	77736071	718	562	20	33	−1.55
139	STRAP	*Bos taurus*	62751962	556	416	16	51	−1.29
95	ENOSF1	*Bos taurus*	114052721	216	171	8	17	−1.83
59	LAP3	*Bos taurus*	165905571	439	319	17	37	1.21
210	TSTD1	*Sus scrofa*	311255145	146	77	10	32	1.31
26	FKBP4	*Sus scrofa*	285818414	354	226	18	46	1.24
120	PPP1CA	*Equus caballus*	194218527	173	115	9	35	−1.25
44	RPSA	*Sus scrofa*	80971504	970	819	16	55	−1.23
98	VAT1	*Bos taurus*	76671278	339	288	9	22	−1.28
222	APOA4	*Sus scrofa*	47523830	484	322	19	38	1.29
122	FBP	*Sus scrofa*	3288991	326	274	9	25	−1.51
147	ISYNA1	*Bos taurus*	114051253	545	452	15	24	−1.70
31	ISYNA1	*Equus caballus*	194232542	195	136	11	17	1.24
110	DDX39	*Bos taurus*	77736449	488	380	17	37	−1.30
145	HNRNPF	*Sus scrofa*	194042660	1040	795	24	65	−1.23
151	SEPHS1	*Bos taurus*	115496754	844	731	14	47	−1.24
137	MAT2A	*Bos taurus*	155371989	836	662	19	49	1.29
140	AGMAT	*Bos taurus*	194674166	283	245	7	22	1.26
116	PPA1	*Sus scrofa*	194042750	424	284	17	54	−1.20
215	RBBP7	*Canis lupus familiaris*	74006531	536	418	15	41	−1.33
209	CTSB	*Sus scrofa*	171948776	123	94	5	16	−1.66
124	MDH1	*Sus scrofa*	164543	583	449	16	52	−1.27
57	HPD	*Sus scrofa*	47523532	905	737	19	53	−1.21
131	ARG1	*Sus scrofa*	47522912	1090	881	20	60	−1.37

[a] The positions of these spots are displayed in the master gel in Fig. 2.
[b] Detailed list of peptide information was shown in Supplemental Table S7.
[c] Positive values represent up-regulation after treatment; negative values represent down-regulation after treatment.
[d] The identified proteins are grouped according to their functions.

66) were considered confident identifications. The identified proteins were then matched to specific processes or functions by searching Gene Ontology (http://www.geneontology.org/).

Bioinformatics Analysis—An analysis of diseases associated with the genes and proteins altered by T-2 in porcine hepatocyte cells was performed with the text-mining Pathway Studio™ (version 7.0) software (Ariadne Genomics, Inc. Rockville, MD), which uses a database assembled from scientific abstracts and a manually created dictionary of synonyms to recognize biological terms. The changed transcripts and identified proteins were converted to their corresponding homologous gene IDs in humans and imported into Pathway Studio; each identified relationship was confirmed manually with the relevant PubMed/Medline hyperlinked texts.

Vector Construction, Prokaryotic Expression and Purification of Recombinant CYP3A46—For eukaryotic expression, the open reading frame (ORF) region of pig cytochrome P450 3A46 (CYP3A46) (***NM_001134824***), carboxylesterase 1C5 (CES1C5) (***X63323***), and epoxide hydrolase 1 (EPHX1) (***NM_214355***) were cloned and inserted into NotI/HindIII sites, NotI/EcoR I sites, and NotI/HindIII sites of pcDNA™3.1/myc-His(-)A vector (Invitrogen, Carlsbad, CA), respectively. The primers used for plasmids construction (restriction enzyme sites italicized) are as follows, CYP3A46-F: 5′-AAA*GCGGCCGC*CATGGACCTGAT-3′, CYP3A46-R: 5′-CA*AAGCTT*GGCTCCACTTGTGGTCC-3′; CES1C5-F: 5′-AAA*GCGGCCGC*C-ATGGGGCTTCTCCC-3′, CES1C5-R: 5′-GGG*GAATTC*TCAGCTCAGCATGC-TTTATCTTGGG-3′; EPHX1-F: 5′-AAA*GCGGCCGC*CATGGGGCTG-3′, EPHX1-R: 5′-CA*AAGCTT*CTGCTGCTCCAACAGCC-3′, respectively.

To allow functional expression in *Escherichia coli*, the N-terminal coding region of mammalian CYP cDNA requires modification, for which we selected *ompA*+2 according to Cytochrome P450 Protocols (31). In brief, a cDNA fragment encoding the bacterial *ompA* leader sequence (21 amino acid residues) and two additional spacer amino acid residues (Leu-Glu) were fused to the CYP3A46 cDNA by PCR. The fragment of *ompA*-CYP3A46 cDNA-myc-His (myc tag and His tag from pcDNA™3.1/myc-His) was then inserted into NdeI/XbaI sites of pCWOri+ vector. The generated plasmids (pcDNA-CYP3A46, pcDNA-CES1C5, pcDNA-EPHX1, and pCWOri-CYP3A46) were verified by sequencing analyses.

Expression plasmid pCWOri-CYP3A46 was transformed into DH5α. A single clone was grown in LB media with shaking at 37 °C 5–7 h, and then diluted 1:100 in modified TB media (32). When the OD_{600} of the expression culture reached 0.7–0.8, 1 mM of IPTG was added and the expression of recombinant CYP3A46 was induced at 30 °C for 36 h. The detailed methods of CYP3A46 purification are given in the supplemental Data.

S9 Preparation and Western Blot Analysis—Before transfection, HepG2 cells (ATCC No. HB-8065) were grown overnight to 80% confluence in 6-well plates. For each well, 4 μg of the expression constructs (pcDNA-CYP3A46, pcDNA-CES1C5, pcDNA-EPHX1, or empty vector) were mixed with 10 μl of Lipofectamine 2000 (Invitrogen) in 500 μl of FBS-free DMEM. Transfections were performed in 800 μl of FBS-free DMEM for 6 h. Forty-eight hours after transfection, the cells were selected by 500 μg/ml of Geneticin (G418, Amresco, Solon, OH). After about one month, surviving colonies (termed

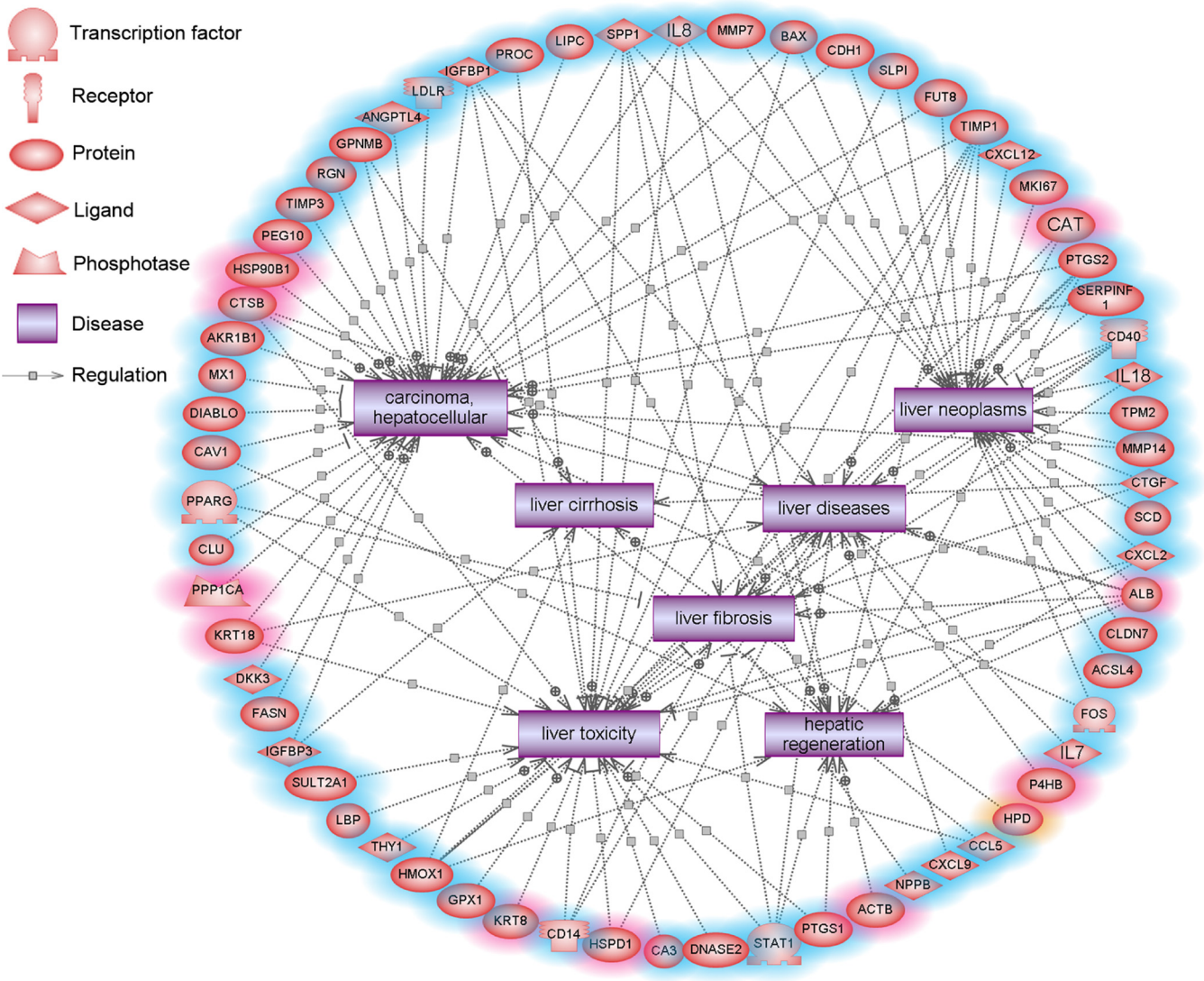

FIG. 3. **Pathway mapping of altered gene and protein expression in porcine hepatocytes treated with 0. 05 μg/ml of T-2 using Pathway Studio.** The network indicated many genes and proteins involved in liver injury and diseases. Nodes with a *red* shadow indicate genes were changed in two-dimensional DIGE, nodes with a *blue* shadow indicate the molecules were changed in microarray, and *orange* indicates the genes were altered in both. MMP7, matrix metallopeptidase 7; BAX, BCL2-associated X protein; CDH1, cadherin 1; SLPI, secretory leukocyte peptidase inhibitor; FUT8, fucosyltransferase 8; TIMP1, TIMP metallopeptidase inhibitor 1; CXCL12, chemokine (C-X-C motif) ligand 12; MKI67, antigen identified by monoclonal antibody K_i-67; CAT, catalase; PTGS2, prostaglandin-endoperoxide synthase 2; SERPINF1, serpin peptidase inhibitor, clade F, member 1; CD40, CD40 molecule, TNF receptor superfamily member 5; IL18, interleukin 18; TPM2, tropomyosin 2; MMP14, matrix metallopeptidase 14; CTGF, connective tissue growth factor; SCD, stearoyl-CoA desaturase; CXCL2, chemokine (C-X-C motif) ligand 2; ALB, albumin; CLDN7, claudin 7; ACSL4, acyl-CoA synthetase long-chain family member 4; FOS, v-fos FBJ murine osteosarcoma viral oncogene homolog; IL7, interleukin 7; P4HB, prolyl 4-hydroxylase, beta polypeptide; HPD, 4-hydroxyphenylpyruvate dioxygenase; CCL5, chemokine (C-C motif) ligand 5; CXCL9, chemokine (C-X-C motif) ligand 9; NPPB, natriuretic peptide precursor B; ACTB; actin, beta; PTGS1, prostaglandin-endoperoxide synthase 1; STAT1, signal transducer and activator of transcription 1, 91kDa; DNASE2, deoxyribonuclease II, lysosomal; CA3, carbonic anhydrase III, muscle specific HSPD1, heat shock 60kDa protein 1; CD14, CD14 molecule; KRT8, keratin 8; GPX1, glutathione peroxidase 1; HMOX1, heme oxygenase 1; THY1, Thy-1 cell surface antigen; LBP, lipopolysaccharide binding protein; SULT2A1, sulfotransferase family, cytosolic, 2A, dehydroepiandrosterone (DHEA)-preferring, member 1; IGFBP3, insulin-like growth factor binding protein 3; FASN, fatty acid synthase; DKK3, dickkopf homolog 3; KRT18, keratin 18; PPP1CA, protein phosphatase 1, catalytic subunit, alpha isoform; CLU, clusterin; PPARG, peroxisome proliferator-activated receptor gamma; CAV1, caveolin 1, caveolae protein, 22kDa; DIABLO, diablo homolog; MX1, myxovirus resistance 1, interferon-inducible protein p78; AKR1B1, aldo-keto reductase family 1, member B1; CTSB, cathepsin B; HSP90B1, heat shock protein 90kDa beta, member 1; PEG10, paternally expressed 10; TIMP3, TIMP metallopeptidase inhibitor 3; RGN, regucalcin; GPNMB, glycoprotein nmb; ANGPTL4, angiopoietin-like 4; LDLR, low density lipoprotein receptor; IGFBP1, insulin-like growth factor binding protein 1; PROC, protein C; LIPC, lipase, hepatic; SPP1, secreted phosphoprotein 1; IL8, interleukin 8.

HepG2-pcDNA, HepG2-CYP3A46, HepG2-CES1C5, and HepG2-EPHX1) were harvested as a pool and propagated in medium containing 200 μg/ml of G418.

The HepG2 transformants grown in culture medium containing G418 (200 μg/ml) were first rinsed with phosphate buffered saline (PBS, PH 7.4), scraped, and collected in homogenization buffer containing 0.1 M of Tris-HCl pH 7.5, and then sonicated five times at 40 W for 5 s with 10 s intervals. The resulting homogenate was centrifuged at 9000 × *g* at 4 °C for 20 min to isolate the S9 fraction, which was then transferred carefully to a clean tube for Western blot analysis or enzyme activity assay. As S9 fractions contain cytosol and microsomes, they are frequently used in assays to measure metabolism of drugs and other xenobiotics. Protein concentrations in S9 fractions were estimated by the Bradford method.

Proteins from the S9 fractions of HepG2 transformants or *E. coli* were separated on 10% SDS-PAGE gels and then electrophoretically transferred to a PVDF membrane (PALL, Ann Arbor, MI). The membrane was blocked with freshly prepared Tris-buffered saline/Tween 20 (TBST) buffer (25 mM of Tris-HCl pH 7.5, 150 mM of NaCl and 0.1% Tween-20) containing 5% nonfat dry milk for 1 h at room temperature, incubated for 1 h with primary antibody in TBST buffer containing 1% milk, washed three times with TBST, each for 10 min, incubated with secondary antibody for 1 h at room temperature and then washed for another 30 min with TBST buffer. Band detection was performed using the LumiGLO® Chemiluminescent Substrate Kit (CST, Beverly, MA), according to manufacturer's instructions. The antibodies and markers used were as follows: β-actin (C4) (sc-47778, Santa Cruz Biotechnology, Santa Cruz, CA) at 1:1000; c-myc (9E10) (sc-40, Santa Cruz Biotechnology) at 1:500; HRP-rabbit anti-mouse IgG (Gamma) (Invitrogen) at 1:4000; and biotinylated protein ladder (CST).

Recombinant CYP3A46, CES1C5, and EPHX1 Activity Assays—The T-2 (or HT-2)-metabolizing activities of recombinant CYP3A46, CES1C5 and EPHX1 were determined by incubating T-2 (or HT-2) with the S9 fractions from HepG2-CYP3A46, HepG2-CES1C5, and HepG2-EPHX1 (S9 fraction from HepG2-pcDNA was used as the control) in 5-ml amber glass vials at 37 °C. The incubation mixture contained 4 μg of T-2 (or HT-2), 0.6 mg of S9 protein (S9 protein inactivated by heating for 10 min was used as the control), 0.5 μM or 5 μM of ketoconazole (if needed), 10 mM of $MgCl_2$, 10 mM of KCl, and 0.1 M of Tris-HCl buffer (pH 7.4) in a final volume of 450 μl. After 5 min pre-incubation at 37 °C in a shaking water bath, 1 mM of NADPH was added to start the reaction. At different time points, the reaction was quenched with 2 ml of ice-cold methylene chloride and mixed with a vortex device. The solution was then centrifuged for 10 min at 3000 × *g* at room temperature. Next, 1 ml of the organic layer was transferred to an amber Reacti-vial and dried under a N_2 stream without heating. The residue was redissolved in 100 μl of water/methanol (45:55, v/v) containing 5 mM of ammonium acetate, and used for LC-MS/MS analysis.

The T-2 metabolizing activities of CYP3A46 were further determined by incubating T-2 with purified CYP3A46 protein. The activity of purified CYP3A46 protein was first confirmed by incubating with nifedipine, a specific substrate of CYP3As (33). The incubation mixture contained 0.1 μM of CYP3A46 (proteins inactivated by heating for 10 min was used as the control), 1 μM of ketoconazole (if needed), 0.2 μM of NADPH-P450 reductase, 0.1 μM of cytochrome b_5, 0.02 mg/ml of sodium cholate, 0.02 mg/ml of liposome (DOPC, DLPC, and PS mixture), 30 mM of $MgCl_2$, 200 μM of nifedipine, and 100 mM of potassium phosphate (pH 7.4) in a final volume of 200 μl. After 5 min pre-incubation at 37 °C in a shaking water bath, 1 mM of NADPH was added to start the reaction. Details about extractions and detections of the samples can be found elsewhere (34). The T-2 metabolizing activities of CYP3A46 and ketoconazole inhibition assays were carried out as described above, except that nifedipine was replaced by T-2.

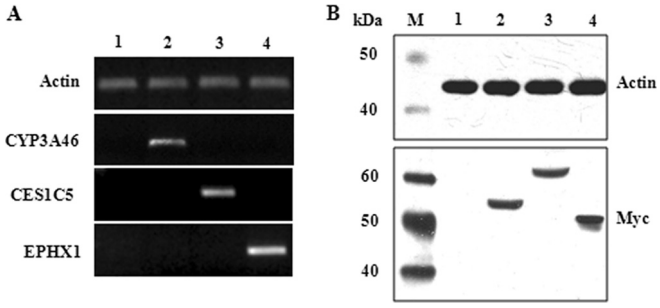

FIG. 4. **Identification of CYP3A46, CES1C5, and EPHX1 stably transfected HepG2 transformants.** RT-PCR (*A*) and Western blotting (*B*) were used to confirm that stable transfections were successful. M, marker; 1, HepG2-pcDNA; 2, HepG2-CYP3A46; 3, HepG2-CES1C5; 4, HepG2-EPHX1.

LC-MS/MS Analyses—The LC-MS/MS analyses were conducted on a rapid resolution liquid chromatography/tandem mass spectrometry (RRLC/MS/MS) system from Agilent Technologies (Waldbronn, Germany) equipped with an electrospray ionization (ESI) interface. Chromatographic separation was carried out on a ZORBAX Eclipse Plus C18 column (100 mm × 2.1 mm, 1.8 μm). Eluent A was water, containing 5 mM of ammonium acetate and eluent B was ACN. The elution was performed by changing the mobile phase composition as follows; after holding at 20% for 5 min, eluent B was increased to 65% in 1 min, further increased to 80% in 4 min, and then kept constant for 4 min. For column re-equilibration, eluent B was decreased to 20% in 1 min and then kept constant for 14 min. The flow rate of the mobile phase was 0.2 ml/min, whereas the injection volume was 2 μl.

For ESI, conditions were set as follows: temperature, 350 °C; nebulizer gas, 20 psi; the ion spray voltage, 4000 V; and collision energy (CE), 10 V. Measurements were performed with multiple reaction monitoring (MRM) in the positive mode, using the parameters listed in supplemental Table S2.

RESULTS

Transcriptome Analysis—To identify gene expression changes associated with T-2, cDNA microarray analysis was performed using mRNA isolated from the control and 0.05 μg/ml T-2 treated primary hepatocytes. Results showed that T-2 changed the mRNA expression profile on swine hepatocytes obviously (supplemental Fig. S1). The transcriptome showed that 1193 transcripts were differentially expressed twofold or greater ($p < 0.05$) in response to 0.05 μg/ml of T-2. Of these, 562 genes were induced and 631 were suppressed. The lists of genes whose expressions were significantly regulated by T-2 are presented in supplemental Table S3 (up-regulated) and supplemental Table S4 (down-regulated). Annotation of genes using the Gene Ontology (GO) database showed that T-2 reaction genes were involved in a variety of biological processes. The largest group of altered genes was associated with oxidation and reduction reaction, whereas immune response, transport, proteolysis, cell adhesion, lipid metabolism process, and apoptosis were the next most commonly annotated groups (all of the listed GO terms with $p < 0.01$) (supplemental Fig. S2A). Changed genes associated with xenobiotic metabolism, lipid metabolism, stress response, and apoptosis are listed separately (Table I).

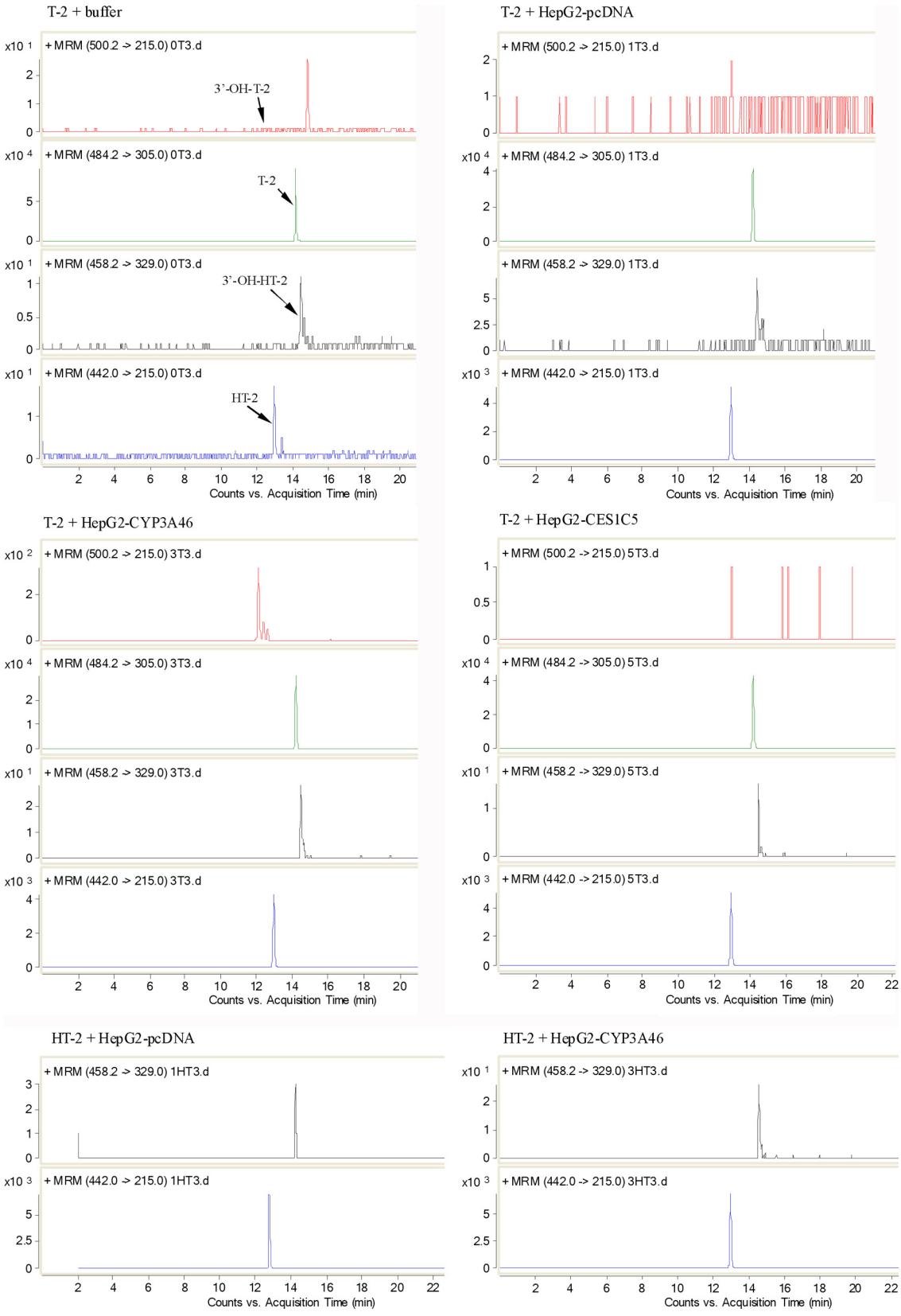
T-2 + buffer
+ MRM (500.2 -> 215.0) 0T3.d
3'-OH-T-2
+ MRM (484.2 -> 305.0) 0T3.d
T-2
+ MRM (458.2 -> 329.0) 0T3.d
3'-OH-HT-2
+ MRM (442.0 -> 215.0) 0T3.d
HT-2
Counts vs. Acquisition Time (min)
T-2 + HepG2-pcDNA
+ MRM (500.2 -> 215.0) 1T3.d
+ MRM (484.2 -> 305.0) 1T3.d
+ MRM (458.2 -> 329.0) 1T3.d
+ MRM (442.0 -> 215.0) 1T3.d
Counts vs. Acquisition Time (min)
T-2 + HepG2-CYP3A46
+ MRM (500.2 -> 215.0) 3T3.d
+ MRM (484.2 -> 305.0) 3T3.d
+ MRM (458.2 -> 329.0) 3T3.d
+ MRM (442.0 -> 215.0) 3T3.d
Counts vs. Acquisition Time (min)
T-2 + HepG2-CES1C5
+ MRM (500.2 -> 215.0) 5T3.d
+ MRM (484.2 -> 305.0) 5T3.d
+ MRM (458.2 -> 329.0) 5T3.d
+ MRM (442.0 -> 215.0) 5T3.d
Counts vs. Acquisition Time (min)
HT-2 + HepG2-pcDNA
+ MRM (458.2 -> 329.0) 1HT3.d
+ MRM (442.0 -> 215.0) 1HT3.d
Counts vs. Acquisition Time (min)
HT-2 + HepG2-CYP3A46
+ MRM (458.2 -> 329.0) 3HT3.d
+ MRM (442.0 -> 215.0) 3HT3.d
Counts vs. Acquisition Time (min)

Effect on Xenobiotics Metabolism Enzymes—Most xenobiotics are metabolized by Phase I enzymes. Using microarray, we demonstrated that exposing porcine hepatocytes to 0.05 μg/ml of T-2 increased mRNA levels of CYP3A46, CYP3A39 (92% identity at amino acid levels between two CYP3A members), and CYP2C42, but decreased CYP2D25 and CYP51 levels (Fig. 1*A*, Table I). Their alterations were further confirmed by real-time PCR analysis (Fig. 1*B*, 1*C*). Hydrolysis is one of the most important metabolic reactions of T-2. Increased mRNA levels of carboxylesterase CES1C4 were also observed in porcine hepatocytes exposed to 0.05 μg/ml of T-2 (Fig. 1*A*, 1*C* and Table I). Epoxide reduction of T-2 was the significant detoxification reaction for T-2. In our microarray assay, the mRNA level of the microsomal epoxide hydrolase gene (EPHX1) increased in porcine hepatocytes treated with T-2 (Fig. 1*A*, 1*C* and Table I).

Proteome Analysis—Porcine hepatocyte proteins in the control and 0.05 μg/ml T-2 treatment groups were labeled with DIGE Fluor dye and separated on a linear IPG strip (pH 4–7) in the first dimension and on a 12.5% SDS-polyacrylamide gel in the second dimension (supplemental Fig. S3). Proteome analysis of primary hepatocytes revealed 260 protein spots whose levels changed significantly (1.2-fold change or greater, $p < 0.05$) in the 0.05 μg/ml T-2 group compared with the control (Fig. 2). One hundred and four protein spots were excised from the silver-stained gels and identified by MALDI-TOF-MS/MS analysis. After a MASCOT database search, 84 different proteins were identified successfully (34 up-regulated and 50 down-regulated) (Table II). According to their biological processes (GO term) (supplemental Fig. S2B), the most common groups of identified proteins included: (1) cytoskeleton proteins, such as plastin 3 (PLS3), annexin A4 (ANXA4), ANXA5, and tubulin alpha-1D chain (TUBA1A); (2) protein binding proteins, such as keratin 18 (KRT18), KRT19, coronin, actin binding protein, and 1B (CORO1B); (3) stress response proteins, such as heat shock 70 kDa protein 1B (HSPA1B), heat shock protein 90 kDa beta member 1 (HSP90B1), 60 kDa heat shock protein, mitochondrial isoform 1 (HSPD1), and catalase (CAT); (4) electron transport proteins, such as NADH dehydrogenase 39 kDa subunit (NDUFA9), NADH-ubiquinone oxidoreductase 75 kDa subunit, mitochondrial precursor (NDUFS1). and cytochrome b-c1 complex subunit 1 (UQCRC1); and (5) lipid metabolic process proteins, such as short/branched chain specific acyl-CoA dehydrogenase, mitochondrial precursor (ACADSB), alpha-aminoadipic semialdehyde dehydrogenase (ALDH7A1), and estradiol 17-beta-dehydrogenase 8 (HSD17B8). One significantly altered spot was identified as porcine CES1C4, which was up-regulated at the mRNA level in the microarray. Another member of the carboxylesterases, CES1C5, also significantly increased in our 2-D DIGE results. Both CES1C5 and CES1C4 belong to the same subfamily of CES1, and shared 96% identity at amino acid levels.

Genes Associated with Hepatic Diseases, Lipid Metabolism, and Oxidative Stress Response—To identify potential changes in cell function, we integrated the transcriptional and proteomic results and analyzed the disease network regulated by the T-2 altered genes using Pathway Studio software. This software uses the ResNet Database, representing different sets of precompiled information on biological relationships and associations as well as facts extracted from the biomedical literature using MedScan (35). Analysis by Pathway Studio revealed many genes involved in hepatic injury and disease (Fig. 3), as well as lipid metabolism (supplemental Fig. S4A) and oxidative stress responses (supplemental Fig. S4B).

Many genes associated with hepatic injury and disease, including liver toxicity, regeneration, fibrosis, cirrhosis, neoplasm, and carcinoma, were altered by T-2 treatment in porcine hepatocytes. For example, tissue inhibitor of metalloproteinase-1 (TIMP-1), an important regulator of matrix metalloproteinase activity, was up-regulated by T-2 treatment. Studies have shown that TIMP-1 levels increase with the development of liver disease, correlating closely with degree of liver fibrosis (36). Clusters of differentiation 14 also increased in T-2 treatment groups. This receptor is necessary for the occurrence of ethanol-induced liver injury, and increased levels of Clusters of differentiation 14 correlate with severity of alcoholic liver disease (37).

Many genes involved in oxidative stress reaction and lipid metabolism were altered by T-2, some of which are involved in the pathogenesis and prognosis of liver disease. For example, heme oxygenase-1 (HMOX-1), which was down-regulated in the T-2 treatment group, encodes for a protein in possession of anti-oxidative characteristics. The HMOX-1 gene plays an important role in many physiological and pathological processes, such as liver ischemia-reperfusion injury, liver transplantation, and acute liver injury (38). Our results also showed that T-2 decreased the expression of peroxisome proliferator-activated receptor gamma (PPARγ), which is an important nuclear receptor for the regulation of fatty acid storage and glucose metabolism. Studies have shown that PPARγ overexpression inhibits the activation of hepatic stellate cells and attenuates liver fibrosis (39), whereas a decrease of PPARγ in porcine hepatocytes may contribute to liver injury and toxicity by T-2.

FIG. 5. **LC-ESI-MS/MS analysis of T-2 (or HT-2) and its metabolites formed in HepG2 transformants expressing CYP3A46 and CES1C5.** T-2 was incubated with buffer or S9 fractions from HepG2-pcDNA, HepG2-CYP3A46, and HepG2-CES1C5 for 3 h, and HT-2 was incubated with S9 fractions from HepG2-pcDNA and HepG2-CYP3A46 for 3 h, then the products were analyzed by LC-ESI-MS/MS. The detection was accomplished by MRM with the transitions *m/z* 484.2/305.0 for T-2, *m/z* 442.0/215.0 for HT-2, *m/z* 500.2/215.0 for 3′-hydroxy-T-2, and *m/z* 458.2/329.0 for 3′-hydroxy-HT-2.

Metabolism of T-2 in HepG2 Cells Expressed Recombinant Phase I Proteins—To confirm whether porcine CYP3A46, CES1C5, and EPHX1 were involved in the biotransformation of T-2 or HT-2, we first obtained HepG2 transformants expressing porcine CYP3A46, CES1C5, and EPHX1. Stable transformants of HepG2 were then tested by RT-PCR and Western blotting. As shown in Fig. 4*A*, stable transfection of full-length cDNAs of porcine CYP3A46, CES1C5, and EPHX1 in HepG2 cells led to significant over-expression of these genes at the mRNA level. In addition, CYP3A46, CES1C5, and EPHX1-myc fusion proteins with estimated molecular masses of 55 kDa, 61 kDa, and 50 kDa, respectively, were specifically recognized by anti-myc antibodies (Fig. 4*B*).

The T-2 (or HT-2)-metabolizing activities of recombinant CYP3A46, CES1C5, and EPHX1 were determined by incubating T-2 (or HT-2) with S9 fractions from HepG2-CYP3A46, HepG2-CES1C5, and HepG2-EPHX1 (S9 fraction from HepG2-pcDNA was used as the control), respectively. We used LC-MS/MS to detect T-2 and its metabolites, with their relative amounts were represented as values of peak area. When T-2 with the S9 protein of HepG2-CYP3A46 was incubated for 0.5 h, we detected 3′-hydroxy-T-2, a newly generated metabolite not detected in the T-2 plus HepG2-pcDNA group (supplemental Table S5). The amount of 3′-hydroxy-T-2 increased from 1186 to 1969 (peak area) as incubation time increased from 0.5 h to 3 h (Fig. 5 and supplemental Table S5). When the HepG2-CYP3A46 S9 protein was inactivated by heating before T-2 incubation, the 3′-hydroxy-T-2 peak disappeared (Table III). When 0.5 μM of ketoconazole which is a potent inhibitor of CYP3A4-mediated metabolism in humans and has been widely used as a probe of CYP3A inhibition in other animal species (40) was added into the reaction system, the generation of 3′-hydroxy-T-2 in the T-2 plus HepG2-CYP3A46 group was notably inhibited (Table III). As the dosage of ketoconazole increased to 5 μM, the amount of 3′-hydroxy-T-2 decreased to 117 (peak area). However, no significant effect was found in the T-2 plus HepG2-pcDNA group when ketoconazole was added. These results reveal that CYP3A46 can catalyze T-2 into 3′-hydroxy-T-2.

Furthermore, another hydroxylation metabolite (3′-hydroxy-HT-2) was detected when incubating T-2 with S9 fractions from HepG2-CYP3A46 (supplemental Table S5). There was no distinct difference in 3′-hydroxy-HT-2 amounts between the T-2 plus HepG2-CYP3A46 group and the T-2 plus HepG2-pcDNA group.

In addition, to study whether porcine CYP3A46 catalyzed HT-2 into 3′-hydroxy-HT-2, we incubated HT-2 with S9 fractions from HepG2-CYP3A46 directly. Compared with the control, a slight increase in the amount of 3′-hydroxy-HT-2 was detected in the HepG2-CYP3A46 group after 3 h incubation with HT-2 (Fig. 5 and Table S6). This was enhanced by inhibiting the activity of CYP3A46 through heating S9 proteins or adding ketoconazole to the reaction systems (Table IV).

TABLE III

T-2 metabolism of CYP3A46. T-2 was incubated with HepG2-pcDNA, HepG2-CYP3A46 (active or inactive), and in the reactions containing ketoconazole (KTZ) or not for 3 h. T-2, HT-2, 3′-hydroxy-T-2, 3′-hydroxy-HT-2 were detected and analyzed by LC-MS/MS. Data are represented as the values of peak area. n.d., not detected

Analyte	T-2								
	Buffer	HepG2-pcDNA	HepG2-CYP3A46	HepG2-CYP3A46 (inactive)	HepG2-pcDNA (0.5 μM KTZ)	HepG2-CYP3A46 (0.5 μM KTZ)	HepG2-pcDNA (5 μM KTZ)	HepG2-CYP3A46 (5 μM KTZ)
T-2	403624	144905	166658	447384	175224	136566	199617	215262
HT-2	96	30397	32197	219	38583	28014	33047	30092
3′-hydroxy-T-2	n.d.	n.d.	5296	n.d.	7	1419	n.d.	117
3′-hydroxy-HT-2	47	30	36	62	28	26	64	62

10.1074/mcp.M111.008748–11

Thus, CYP3A46 was also able to catalyze HT-2 into 3′-hydroxy-HT-2.

Using the same method, we detected whether porcine CES1C5 or EPHX1 was involved in the hydrolysis or de-epoxidation of T-2, respectively. A large amount of HT-2 was detected in the T-2 plus HepG2-CES1C5 group (Fig. 5 and supplemental Table S5). However, a similar amount of HT-2 was detected in the HepG2-pcDNA group (supplemental Table S5). We further tried to detect other hydrolysis metabolites of T-2 or HT-2 such as neosolaniol, T-2 triol and T-2 tetraol in all reactions, whereas none were identified (data not shown).

To confirm whether EPHX1 could de-epoxidate T-2, we attempted to detect the five main de-epoxidation metabolites reported in other research, including deepoxy-HT-2, deepoxy-3′-hydroxy-HT-2, deepoxy-T-2 triol, deepoxy-3′-hydroxy- T-2 triol, and deepoxy-T-2 tetraol. We speculated on the possible tandem mass spectrometry parameters of these metabolites according to the known parameters of T-2 and HT-2 metabolites. No de-epoxidation metabolites in any reaction were detected (data not shown), which implied that EPHX1 was probably not the dominant EPHX responsible for the de-epoxidation reaction of T-2 in porcine primary hepatocytes.

T-2 Metabolism of Purified CYP3A46—To further confirm the role of CYP3A46 in T-2 hydroxylation, we used prokaryotic expression and affinity chromatography to express and purify recombinant CYP3A46 proteins. A myc-His-tagged fusion protein with about 55 kDa was expressed (Fig. 6*A*) (Lane 2 and 3) and purified (Lane 4) successfully (Fig. 6*B*). Nifedipine is a specific substrate of CYP3As and is the standard substrate of CYP3A46 (33). We first tested the bioactivities of purified CYP3A46, using nifedipine as the substrate. As shown in Fig. 6*C*, CYP3A46 transformed nifedipine to its metabolite oxidized nifedipine. This reaction was specifically blocked by ketoconazole (Fig. 6*D*). We further incubated purified CYP3A46 with T-2. A large amount of 3′-hydroxy-T-2 was detected in the T-2 plus purified CYP3A46 group, whereas it was not detected in the T-2 plus buffer group (Fig. 6*E*). When the purified CYP3A46 protein was inactivated by heating before T-2 incubation, the 3′-hydroxy-T-2 peak disappeared. In addition, ketoconazole also inhibited this reaction to a lesser extent.

DISCUSSION

Trichothecenes are a large group of mycotoxins mainly produced by *Fusarium* fungi, with T-2 of particular concern because of its high toxicity and prevalence (22, 41–44). To obtain a detailed understanding of molecular changes that occur in response to T-2, differently expressed liver mRNA and proteins between the 0.05 μg/ml T-2 treatment group and the control were examined by microarray and 2-D DIGE. In general, as microarray and 2-D have limitations, it is better to use an integrated genomic and proteomic approach to study

TABLE IV

HT-2 metabolism of CYP3A46. HT-2 was incubated with HepG2-pcDNA and HepG2-CYP3A46 (active or inactive) in the reactions containing ketoconazole (KTZ) or not for 3 h. HT-2 and 3′-hydroxy-HT-2 were detected and analyzed by LC-MS/MS. Data are represented as the values of peak area

Analyte	HT-2								
	Buffer	HepG2-pcDNA	HepG2-CYP3A46	HepG2-CYP3A46 (inactive)	HepG2-pcDNA (0.5 μM KTZ)	HepG2-CYP3A46 (0.5 μM KTZ)	HepG2-pcDNA (5 μM KTZ)	HepG2-CYP3A46 (5 μM KTZ)
HT-2	55877	37117	16367	65794	39667	49469	44060	58316
3′-hydroxy-HT-2	33	40	223	26	16	9	28	39

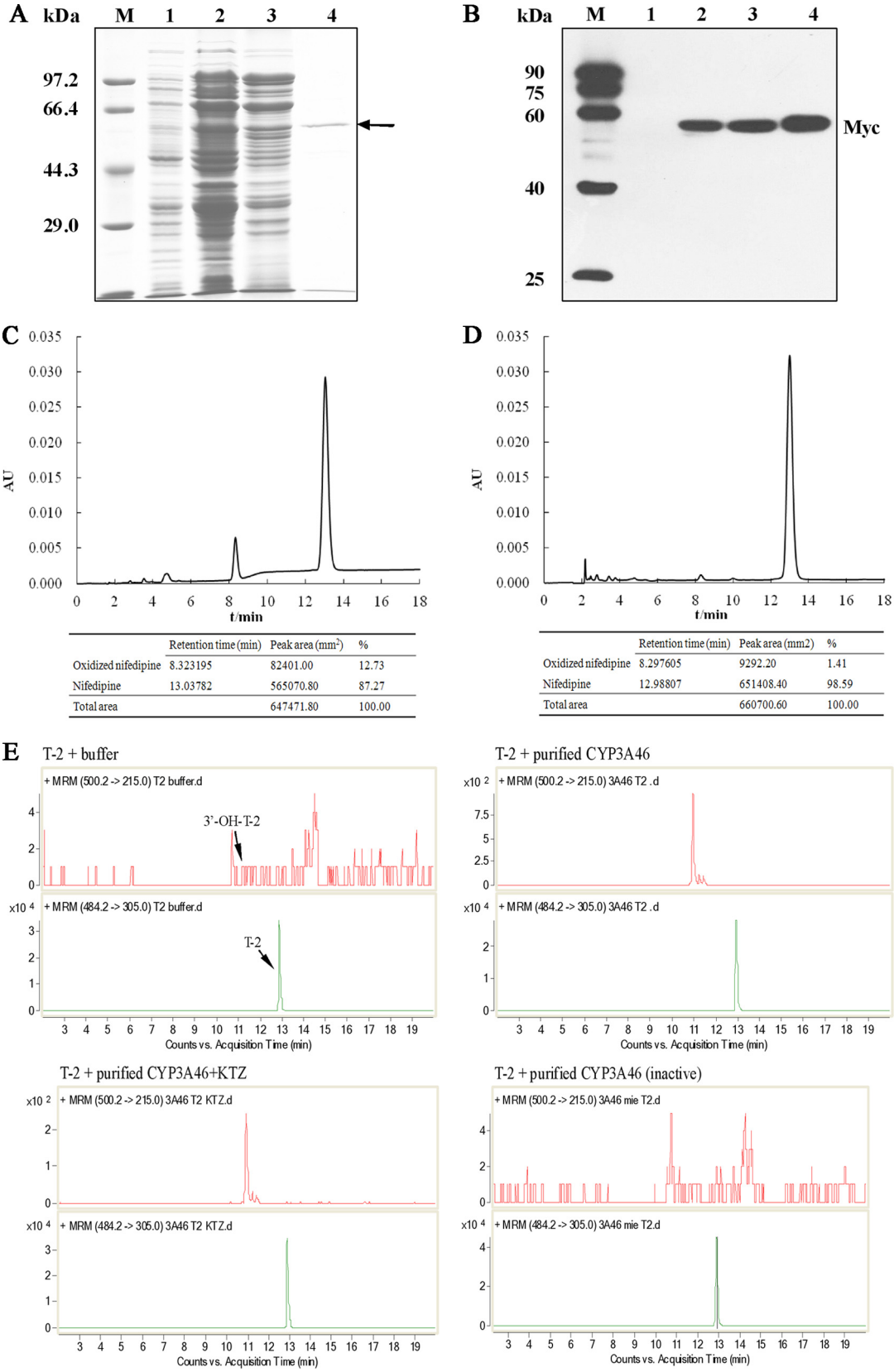

	Retention time (min)	Peak area (mm^2)	%
Oxidized nifedipine	8.323195	82401.00	12.73
Nifedipine	13.03782	565070.80	87.27
Total area		647471.80	100.00

	Retention time (min)	Peak area (mm2)	%
Oxidized nifedipine	8.297605	9292.20	1.41
Nifedipine	12.98807	651408.40	98.59
Total area		660700.60	100.00

the molecular mechanism of T-2 toxicity and its biotransformation at a cellular level. Because gene expression is a complicated process, mRNA and protein abundance are affected by many cellular and physical processes, including transcription, post-transcriptional regulation, RNA degradation and splicing, translation, post-translational modification, and degradation of proteins. Comparative studies of mRNA and protein abundance performed so far indicate that the correlation across large data sets is typically modest (45, 46). In our study, only a few genes were altered simultaneously in both microarray and 2-D DIGE assays, including the Phase I CES enzyme gene CES1C5, fructose-1, 6-bisphosphatase (FBP), 4-hydroxyphenylpyruvate dioxygenase (HPD) and tyrosine 3-monooxygenase/tryptophan 5-monooxygenase activation protein, zeta (YWHAZ).

To provide insight into global gene profiles and identify potential changes in cell function, we integrated the transcriptional and proteomic results and analyzed the disease or cell process network regulated by the T-2 altered genes using Pathway Studio software, which annotates the relationship between genes or proteins and diseases or cell processes through the ResNet database.

The T-2 treatment led to changes in genes associated with lipid metabolism (including lipid degradation, metabolism, lipolyses, and fatty acid biosynthesis) in both transcriptome and proteome analysis. Both hepatic lipase (LIPC) and long-chain acyl-Coenzyme A dehydrogenase (ACADL) were up-regulated in response to T-2 treatment, whereas fatty acid synthase (FASN) decreased. Although the results showed enhancement of lipid catabolism in the T-2 treatment group, they also showed that low density lipoprotein receptor (LDLR) and ACADSB decreased. Three lipid desaturases, specifically fatty acid desaturase 1 (FADS1), FADS2, and stearoyl-CoA desaturase (SCD), also decreased in the T-2 treatment group. The observed imbalance in lipid metabolism by T-2 may impair energy generation and the ability of ROS elimination and, in turn, contribute to the adverse effect of T-2 on hepatocytes.

The expressions of several genes implicated in apoptosis were up-regulated in treatment groups in microarray, such as caspase 1, caspase 15, CD40, and BCL-2 associated X protein (BAX) (Table I). Some researchers believe that T-2 induces oxidative stress, leading to the activation of different pathways and apoptosis (47). Consistent with this speculation, pathway analysis indicated that many genes involved in mitochondrial respiratory function were altered by T-2. Mitochondrial damage or dysfunction potentially contributed to the generation of ROS and lipid peroxidation. Many hepatic genes related to oxidative stress response, such as CAT, glutathione peroxidase 1 (GPX1), HSPD1, and HSP90B1 increased at the protein or mRNA level in the T-2 group compared with the control group. This indicated that T-2 cytotoxicity to primary hepatocytes was at least partially ascribed to ROS and lipid peroxidation.

Most xenobiotics are metabolized by Phase I enzymes, which are then modified by Phase II enzymes. The main Phase I reactions in trichothecene metabolism are hydroxylation, hydrolysis, and de-epoxidation (48). In the present study, several xenobiotic metabolism enzymes, including five cytochrome P450s (CYP3A46, CYP3A39, CYP2C42, CYP2D25, and CYP5), two carboxylesterases (CES1C4 and CES1C5), and an epoxide hydrolase (EPHX1), were altered in porcine hepatocytes exposed to 0.05 μg/ml of T-2. Research has shown that T-2 up- or down-regulates CYP450 expression and biotransformation activities in both animal and human models, and many T-2 hydroxylation products, such as 3′-hydroxy-T-2, 3′-hydroxy-HT-2, 3′-hydroxy-HT-2 triol, 4′-hydroxy-T-2, 4′-hydroxy-HT-2, deepoxy-3′-hydroxy-HT-2, deepoxy-3′-hydroxy-T-2 triol, and 3′-7-dihydroxy-HT-2, have been found in animal liver homogenates (49–51). Studies have also shown CYP1A protein expression decreases in pigs fed 2102 μg/kg of T-2 over 28 days (52). The expression of CYP1A in rats (50) and rabbits (51) is reduced when animals are exposed to high doses of T-2 (0.25 or 1 mg/kg body weight). In our study, however, the mRNA levels of the CYP1A subfamily were similar in the control and T-2 treatment groups. This discrepancy may be because of variance among experimental systems as T-2 toxicity can be affected by factors such as administration route, time of exposure, and dosage (10). Hydrolysis of xenobiotics is one of the most common Phase I metabolic reactions. Carboxylesterases participated in T-2 hydrolysis because hydrolysis was inhibited by eserine and diisopropylfluorophosphate (53). Epoxide reduction of T-2 was a significant detoxification reaction, and de-epoxy T-2 was 400 times less toxic than T-2 in rat skin irritation assay and nontoxic to mice at 60 mg/kg ip (4).

Although the main reactions of T-2 metabolism are hydroxylation, hydrolysis, and de-epoxidation (9), relatively few studies have investigated which molecules are responsible for the biotransformation of T-2 in hepatocytes (23). Porcine CYP3As (CYP3A46 and CYP3A39), CESs (CES1C4 and CES1C5), and EPHX1, which were induced in the T-2 treatment compared with the control, possibly participate in the hydroxylation, deacylation, and de-epoxidation reaction of T-2 in porcine hepatocytes. To investigate the function of

FIG. 6. **T-2 metabolism of purified CYP3A46.** The prokaryotic expression and purified proteins were analyzed by 10% SDS-PAGE gels with Coomassie blue staining (*A*) and Western blotting using anti-myc antibodies (*B*). Lane 1: non-IPTG induced total cell lysates; lane 2: IPTG induced total cell lysates; lane 3: solubilized membrane fraction; lane 4: FPLC purified protein. The bioactivities of purified CYP3A46 were tested by incubating CYP3A46 with nifedipine (*C*) or nifedipine and ketoconazole (*D*). HPLC was used to detect nifedipine and its metabolite. *E*, Purified CYP3A46 was further incubated with T-2, and then the products were analyzed by LC-ESI-MS/MS. The detection was accomplished by MRM with the transitions *m/z* 484.2/305.0 for T-2, and *m/z* 500.2/215.0 for 3′-hydroxy-T-2.

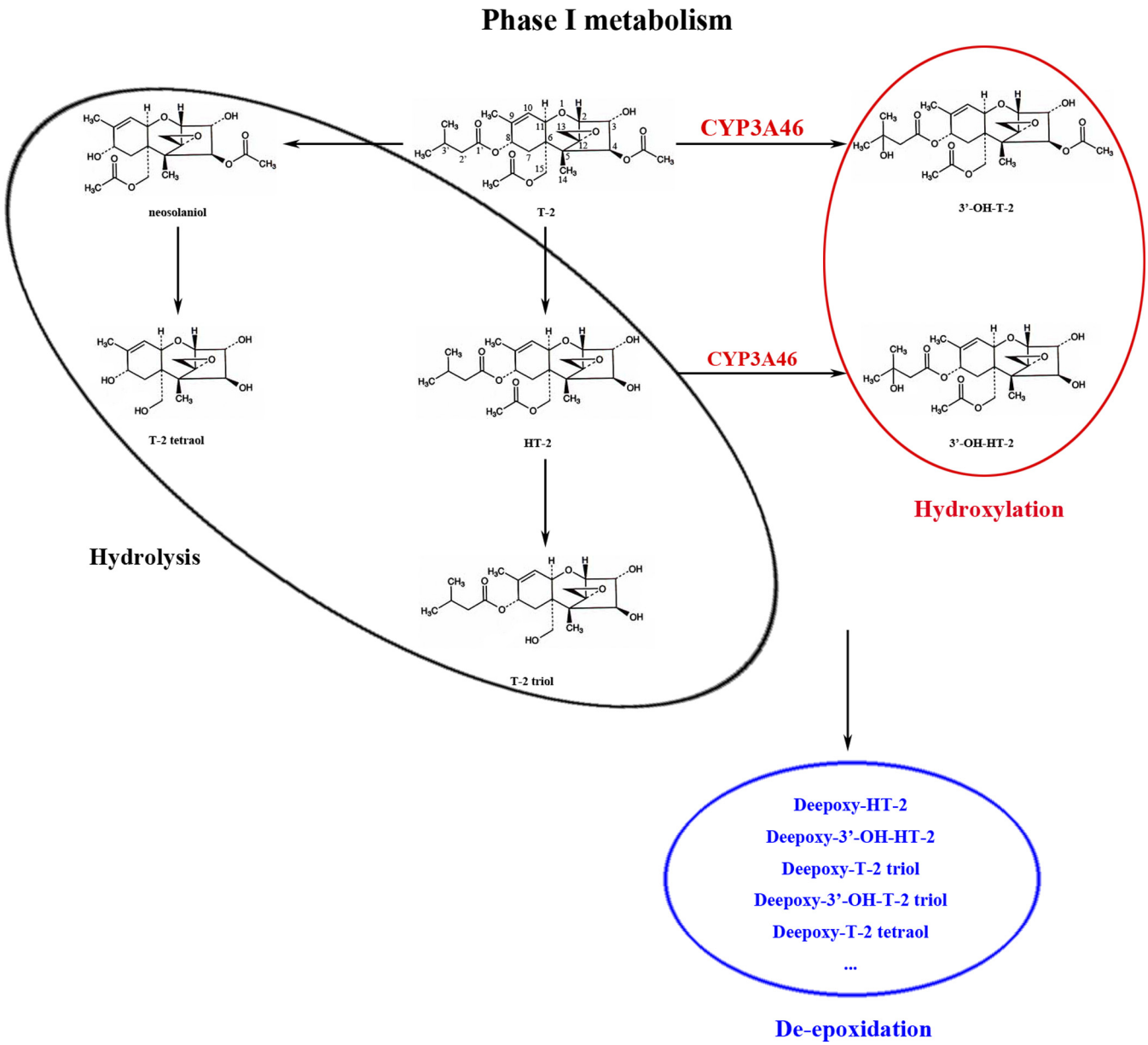

FIG. 7. **Proposed enzymatic systems responsible to the hydrolysis, hydroxylation, and de-epoxidation reaction of T-2 in porcine hepatocytes.** CYP3A46 mainly catalyzed T-2 into 3′-hydroxy-T-2, and also partially catalyzed HT-2 into 3′-hydroxy-HT-2.

these inducible Phase I enzymes in the biotransformation of T-2, the metabolites of T-2 were detected by RRLC/MS/MS in the microsomes of the HepG2 cells transfected to stably expressed recombinant porcine CYP, CES, and EPHX proteins. For CYPs, we focused on the CYP3A subfamily, whose enzymes constitute the most abundant CYPs in the liver and intestine, and are responsible for the oxidative metabolism of many endogenous and xenobiotic compounds, such as toxins, carcinogens, bile acids, and more than half the clinical drugs used today (54, 55). In humans, at least five CYP3A subfamily members have been identified (CYP3A3, CYP3A4, CYP3A5, CYP3A7, and CYP3A43) (56), among which CYP3A4 is the most abundant in the liver and is involved in the metabolism of about 50% of currently marketed therapeutics (54). Porcine CYP3A46 and CYP3A39 share more than 80% amino acid identity with human CYP3A4 (57) and show high homology with CYP 3A4 in some key active sites (58). Amino acid sequence analysis revealed that porcine CYP3A46 and CYP3A39 shared 92% identity at amino acid levels. Therefore only CYP3A46 was selected from the two members of CYP3A (CYP3A46 and CYP3A39) for further *in vitro* biochemistry assays. After incubation with T-2, the S9 protein of HepG2-CYP3A46 yielded a large amount of 3′-hydroxy-T-2, although this reaction was inhibited by adding the potent CYP3A inhibitor, ketoconazole, to the S9 protein. The results clearly revealed that CYP3A46 catalyzed T-2 into 3′-hydroxy-T-2.

Using the same methods, we found that CYP3A46 also slightly catalyzed HT-2 into 3′-hydroxy-HT-2. Furthermore, we performed *in vitro* reactions using purified CYP3A46 protein and confirmed that CYP3A46 played an important role in T-2 hydroxylation. Our present work indicates that CYP3A46 had similar functions with CYP3A4 (34), and it may be the counterpart of CYP3A4 in pigs and the active sites may be involved in T-2 hydroxylation by CYP3A46.

The CYP2C enzymes comprise ~20% of the total CYPs in humans. Porcine CYP2C42, which increased after T-2 treatment, shared 81% similarity to human CYP2Cs (59). Further investigation on the function of the porcine CYP2C42 gene using *in vitro* biochemistry assay was not conducted because of the relatively small change after T-2 treatment compared with the CYP3As. However, we cannot exclude that CYP2C42 may be involved in the transformation of T-2 in porcine hepatocytes.

For CESs, CES1C5 and CES1C4 belonged to the same subfamily of CES1, and shared 96% identity at the amino acid level. Only CES1C5 was selected from the two members of CES1 for further *in vitro* biochemistry assay. As with previous research (48) our *in vitro* results confirmed that T-2 rapidly transformed into HT-2 by S9 proteins from HepG2. However, CES1C5 may not be the dominant enzyme catalyzing this reaction as ester hydrolysis products of T-2 or HT-2 were similar between the control and HepG2-CES1C5 groups. Carboxylesterases have the highest levels of activity in liver microsomes, and are separated into at least five different subfamilies (CES1–5) (60, 61). The increased carboxylesterases in the present study, specifically porcine CES1C4 and CES1C5, shared 96% identity at the amino acid level and belonged to the same isoenzyme subfamily (CES1C). Furthermore, previous research has shown that acetylcholinesterases are more likely the causal agents of T-2 deacetylation than general nonspecific esterases (62), which may be why no difference was observed in the hydrolysis reaction between recombinant CES1C5 and the control group. Similar to CES1C5, no detectable increase in de-epoxidation products was observed in the HepG2-EPHX1 group, suggesting that EPHX1 was not the dominant EPHX responsible for T-2 de-epoxidation. The de-epoxidation of T-2 (or HT-2) may be carried out by intestinal microbes in some species, such as rats and chickens (4, 63), whereas the de-epoxy products detected in some animals comes from intestinal microbes indirectly. We cannot exclude, however, the possibility that trace amounts of de-epoxidation metabolites were lost in the extraction process or that other undetected de-epoxidation metabolites existed in the system.

CONCLUSION

We combined genome array and 2-D DIGE assays to study the effect of T-2 on porcine hepatocytes, which included lipid metabolism disorder, oxidative stress, and apoptosis. Furthermore, Phase I enzymes, including CYP3As, CESs, and EPHX, which may be responsible for hydroxylation, hydrolysis, and de-epoxidation of T-2, were induced by T-2 treatment. Using recombinant proteins in HepG2 cells and purified CYP3A46 proteins, we validated that porcine CYP3A46 mainly catalyzed T-2 to form 3′-hydroxy-T-2. Although it was not its crucial function, CYP3A46 also transformed HT-2 into 3′-hydorxy-HT-2, which facilitated the removal of these toxins from the body (Fig. 7). Two members of the CES1C subfamily and one EPHX were induced in the 0.05 μg/ml T-2 treatment group for primary porcine hepatocytes; however, they were not responsible for the hydrolysis and de-epoxidation of T-2.

* This work was supported by the National Basic Research Program of China (973; Grant: 2009CB118802), the National Natural Science Foundation of China (Grant: 31025006 and 21007069) and the Program for New Century Excellent Talents in University (No. NCET-08-0643).

[S] This article contains supplemental Data, Figs. S1 to S4 and Tables S1 to S7.

** To whom correspondence should be addressed: Dai JY, Key Laboratory of Animal Ecology and Conservation Biology, Institute of Zoology, Chinese Academy of Sciences, Beijing, 100101, P.R. China. Tel.: +86-10-64807185; E-mail: daijy@ioz.ac.cn; Deng YQ, College of Life Sciences, South China Agricultural University, Guangzhou, 510642, P.R. China. Tel.: +86-20-38604967; E-mail: yqdeng@scau.edu.cn.

‡‡ These authors contributed equally to this paper.

REFERENCES

1. Desjardins, A. E., Hohn, T. M., and McCormick, S. P. (1993) Trichothecene biosynthesis in *Fusarium* species: Chemistry, genetics, and significance. *Microbiol. Rev.* **57,** 595–604
2. EU (2001) Opinion of the Scientific Committee on Food on Fusarium Toxins Part 5: T-2 Toxin and HT-2 Toxin. *Scientific Committee on Food (SCF)*
3. Swanson, S. P., Nicoletti, J., Rood, H. D., Jr., Buck, W. B., Cote, L. M., and Yoshizawa, T. (1987) Metabolism of three trichothecene mycotoxins, T-2 toxin, diacetoxyscirpenol and deoxynivalenol, by bovine rumen microorganisms. *J. Chromatogr.* **414,** 335–342
4. Swanson, S. P., Helaszek, C., Buck, W. B., Rood, H. D., Jr., and Haschek, W. M. (1988) The role of intestinal microflora in the metabolism of trichothecene mycotoxins. *Food Chem. Toxicol.* **26,** 823–829
5. Yagen, B., and Bialer, M. (1993) Metabolism and pharmacokinetics of T-2 toxin and related trichothecenes. *Drug Metab. Rev.* **25,** 281–323
6. Klötzel, M., Gutsche, B., Lauber, U., and Humpf, H. U. (2005) Determination of 12 type A and B trichothecenes in cereals by liquid chromatography-electrospray ionization tandem mass spectrometry. *J. Agric. Food Chem.* **53,** 8904–8910
7. Schollenberger, M., Müller, H. M., Rüfle, M., Suchy, S., Plank, S., and Drochner, W. (2006) Natural occurrence of 16 *Fusarium* toxins in grains and feed stuffs of plant origin from Germany. *Mycopathologia* **161,** 43–52
8. Sudakin, D. L. (2003) Trichothecenes in the environment: Relevance to human health. *Toxicol. Lett.* **143,** 97–107
9. Eriksen, G. S., and Pettersson, H. (2004) Toxicological evaluation of trichothecenes in animal feed. *Anim. Feed Sci. Tech.* **114,** 205–239
10. Sokolović, M., Garaj-Vrhovac, V., and Simpraga, B. (2008) T-2 toxin: Incidence and toxicity in poultry. *Arh. Hig. Rada. Toksikol.* **59,** 43–52
11. Schothorst, R. C., and Egmond, H. P. (2004) Report from SCOOP task 3.2.10 "collection of occurrence data of *Fusarium* toxins in food and assessment of dietary intake by the population of EU member states" Subtask: Trichothecenes. *Toxicol. Lett.* **153,** 133–143
12. Pestka, J. J., Zhou, H. R., Moon, Y., and Chung, Y. J. (2004) Cellular and molecular mechanisms for immune modulation by deoxynivalenol and other trichothecenes unraveling a paradox. *Toxicol. Lett.* **153,** 61–73
13. Rizzo, A. F., Atroshi, F., Ahotupa, M., Sankari, S., and Elovaara, E. (1994) Protective effect of antioxidants against free radical-mediated lipid per-

oxidation induced by DON or T-2 toxin. *Zentralbl Veterinarmed A* **41,** 81–90
14. Li, M., Harkema, J. R., Islam, Z., Cuff, C. F., and Pestka, J. J. (2006) T-2 toxin impairs murine immune response to respiratory reovirus and exacerbates viral bronchiolitis. *Toxicol. Appl. Pharmacol.* **217,** 76–85
15. Bunner, D. L., and Morris, E. R. (1988) Alteration of multiple cell membrane functions in L-6 myoblasts by T-2 toxin: An important mechanism of action. *Toxicol. Appl. Pharmacol.* **92,** 113–121
16. Kamalavenkatesh, P., Vairamuthu, S., Balachandran, C., Manohar, B. M., and Raj, G. D. (2005) Immunopathological effect of the mycotoxins cyclopiazonic acid and T-2 toxin on broiler chicken. *Mycopathologia* **159,** 273–279
17. Bouaziz, C., Sharaf El Dein, O., El Golli, E., Abid-Essefi, S., Brenner, C., Lemaire, C., and Bacha, H. (2008) Different apoptotic pathways induced by zearalenone, T-2 toxin and ochratoxin A in human hepatoma cells. *Toxicology* **254,** 19–28
18. Trusal, L. R. (1986) Metabolism of T-2 mycotoxin by cultured cells. *Toxicon* **24,** 597–603
19. Corley, R. A., Swanson, S. P., Gullo, G. J., Johnson, L., Beasley, V. R., and Buck, W. B. (1986) Disposition of T-2 toxin, a trichothecene mycotoxin, in intravascularly dosed swine. *J. Agric. Food Chem.* **34,** 868–875
20. Ellison, R. A., and Kotsonis, F. N. (1974) In vitro metabolism of T-2 toxin. *Appl. Microbiol.* **27,** 423–424
21. Ohta, M., Ishii, K., and Ueno, Y. (1977) Metabolism of trichothecene mycotoxins I. *J. Biochem.* **82,** 1591–1598
22. Wu, Q., Dohnal, V., Huang, L., Kuca, K., and Yuan, Z. (2010) Metabolic pathways of trichothecenes. *Drug Metab. Rev.* **42,** 250–267
23. He, J., Zhou, T., Young, J. C., Boland, G. J., and Scott, P. M. (2010) Chemical and biological transformations for detoxification of trichothecene mycotoxins in human and animal food chains: A review. *Trends in Food Sci. Technol.* **21,** 67–76
24. Donato, M. T., Castell, J. V., and Gómez-Lechón, M. J. (1999) Characterization of drug metabolizing activities in pig hepatocytes for use in bioartificial liver devices: Comparison with other hepatic cellular models. *J. Hepatol.* **31,** 542–549
25. Heijne, W. H., Kienhuis, A. S., van Ommen, B., Stierum, R. H., and Groten, J. P. (2005) Systems toxicology: applications of toxicogenomics, transcriptomics, proteomics and metabolomics in toxicology. *Expert Rev. Proteomics* **2,** 767–780
26. Nzoughet, J. K., Hamilton, J. T., Botting, C. H., Douglas, A., Devine, L., Nelson, J., and Elliott, C. T. (2009) Proteomics identification of azaspiracid toxin biomarkers in blue mussels, *Mytilus edulis. Mol. Cell Proteomics.* **8,** 1811–1822
27. Bae, W., and Chen, X. (2004) Proteomic study for the cellular responses to Cd^{2+} in *Schizosaccharomyces pombe* through amino acid-coded mass tagging and liquid chromatography tandem mass spectrometry. *Mol. Cell Proteomics.* **3,** 596–607
28. Seglen, P. O. (1976) Preparation of isolated rat liver cells. *Methods Cell Biol.* **13,** 29–83
29. Ge, X. H., Wang, J. P., Liu, J., Jiang, J., Lin, H. N., Wu, J., Ouyang, M., Tang, H. Q., Zheng, M., Liao, M., and Deng, Y. Q. (2010) The catalytic activity of cytochrome P450 3A22 is critical for the metabolism of T-2 toxin in porcine reservoirs. *Catal. Comm.* **12,** 71–75
30. Livak, K. J., and Schmittgen, T. D. (2001) Analysis of relative gene expression data using real-time quantitative PCR and the 2(-Delta Delta C(T)) method. *Methods* **25,** 402–408
31. Phillips, I. R., and Shephard, E. A. (2005) Cytochrome P450 Protocols, 2nd Edition. *Methods in Molecular Biology* **320,** 21–22
32. Fisher, C. W., Shet, M. S., Caudle, D. L., Martin-Wixtrom, C. A., and Estabrook, R. W. (1992) High-level expression in *Escherichia coli* of enzymatically active fusion proteins containing the domains of mammalian cytochromes P450 and NADPH-P450 reductase flavoprotein. *Proc. Natl. Acad. Sci. U.S.A.* **89,** 10817–10821
33. Sohl, C. D., Cheng, Q., and Guengerich, F. P. (2009) Chromatographic assays of drug oxidation by human cytochrome P450 3A4. *Nat. Protoc.* **4,** 1252–1257
34. Jiang, J., Wang, J. P., Cai, H., Li, K. B., and Deng, Y. Q. (2011) CYP3As catalyze nifedipine oxidation in pig liver microsomes: Enzyme kinetics, inhibition and functional expression. *Catal. Comm.* **12,** 694–697
35. Nikitin, A., Egorov, S., Daraselia, N., and Mazo, I. (2003) Pathway studio-the analysis and navigation of molecular networks. *Bioinformatics* **19,** 2155–2157
36. Murawaki, Y., Ikuta, Y., Idobe, Y., Kitamura, Y., and Kawasaki, H. (1997) Tissue inhibitor of metalloproteinase-1 in the liver of patients with chronic liver disease. *J. Hepatol.* **26,** 1213–1219
37. Yin, M., Bradford, B. U., Wheeler, M. D., Uesugi, T., Froh, M., Goyert, S. M., and Thurman, R. G. (2001) Reduced early alcohol-induced liver injury in CD14-deficient mice. *J. Immunol.* **166,** 4737–4742
38. Sass, G., Soares, M. C., Yamashita, K., Seyfried, S., Zimmermann, W. H., Eschenhagen, T., Kaczmarek, E., Ritter, T., Volk, H. D., and Tiegs, G. (2003) Heme oxygenase-1 and its reaction product, carbon monoxide, prevent inflammation-related apoptotic liver damage in mice. *Hepatology* **38,** 909–918
39. Yang, L., Chan, C. C., Kwon, O. S., Liu, S., McGhee, J., Stimpson, S. A., Chen, L. Z., Harrington, W. W., Symonds, W. T., and Rockey, D. C. (2006) Regulation of peroxisome proliferator-activated receptor-gamma in liver fibrosis. *Am. J. Physiol. Gastrointest Liver Physiol.* **291,** G902-G911
40. Thummel, K. E., and Wilkinson, G. R. (1998) In vitro and *in vivo* drug interactions involving human CYP3A. *Annu. Rev. Pharmacol. Toxicol.* **38,** 389–430
41. Voyksner, R. D., Hagler, W. M., Jr., and Swanson, S. P. (1987) Analysis of some metabolites of T-2 toxin, diacetoxyscirpenol and deoxynivalenol, by thermospray high-performance liquid chromatography-mass spectrometry. *J. Chromatogr.* **394,** 183–199
42. Yoshizawa, T., Swanson, S. P., and Mirocha, C. J. (1980) T-2 metabolites in the excreta of broiler chickens administered 3H-labeled T-2 toxin. *Appl. Environ. Microb.* **38,** 1172–1177
43. Pittet, A. (1998) Natural occurrence of mycotoxins in foods and feeds: An updated review. *Rev. Med. Vet.* **149,** 479–492
44. Königs, M., Mulac, D., Schwerdt, G., Gekle, M., and Humpf, H. U. (2009) Metabolism and cytotoxic effects of T-2 toxin and its metabolites on human cells in primary culture. *Toxicology* **258,** 106–115
45. Chen, G., Gharib, T. G., Huang, C. C., Taylor, J. M., Misek, D. E., Kardia, S. L., Giordano, T. J., Iannettoni, M. D., Orringer, M. B., Hanash, S. M., and Beer, D. G. (2002) Discordant protein and mRNA expression in lung adenocarcinomas. *Mol. Cell Proteomics* **1,** 304–313
46. Griffin, T. J., Gygi, S. P., Ideker, T., Rist, B., Eng, J., Hood, L., and Aebersold, R. (2002) Complementary profiling of gene expression at the transcriptome and proteome levels in *Saccharomyces cerevisiae. Mol. Cell Proteomics* **1,** 323–333
47. Chaudhari, M., Jayaraj, R., Bhaskar, A. S., and Lakshmana Rao, P. V. (2009) Oxidative stress induction by T-2 toxin causes DNA damage and triggers apoptosis via caspase pathway in human cervical cancer cells. *Toxicology* **262,** 153–161
48. Wu, Q., Dohnal, V., Huang, L., Kuca, K., and Yuan, Z. (2010) Metabolic pathways of trichothecenes. *Drug Metab. Rev.* **42,** 250–267
49. Kobayashi, J., Horikoshi, T., Ryu, J. C., Tashiro, F., Ishii, K., and Ueno, Y. (1987) The cytochrome P-450-dependent hydroxylation of T-2 toxin in various animal species. *Food Chem. Toxicol.* **25,** 539–544
50. Galtier, P., Paulin, F., Eeckhoutte, C., and Larrieu, G. (1989) Comparative effects of T-2 toxin and diacetoxyscirpenol on drug metabolizing enzymes in rat tissues. *Food Chem. Toxicol.* **27,** 215–220
51. Guerre, P., Eeckhoutte, C., Burgat, V., and Galtier, P. (2000) The effects of T-2 toxin exposure on liver drug metabolizing enzymes in rabbit. *Food Addit. Contam.* **17,** 1019–1026
52. Meissonnier, G. M., Laffitte, J., Raymond, I., Benoit, E., Cossalter, A. M., Pinton, P., Bertin, G., Oswald, I. P., and Galtier, P. (2008) Subclinical doses of T-2 toxin impair acquired immune response and liver cytochrome P450 in pigs. *Toxicology* **247,** 46–54
53. Ohta, M., Matsumoto, H., and Ishii, K. (1978) Metabolism of trichothecene mycotoxins II. *J. Biochem.* **84,** 697–706
54. Guengerich, F. P. (1999) Cytochrome P-450 3A4: Regulation and role in drug metabolism. *Annu. Rev. Pharmacol. Toxicol.* **39,** 1–17
55. van Herwaarden, A. E., Wagenaar, E., van der Kruijssen, C. M., van Waterschoot, R. A., Smit, J. W., Song, J. Y., van der Valk, M. A., van Tellingen, O., van der Hoorn, J. W., Rosing, H., Beijnen, J. H., and Schinkel, A. H. (2007) Knockout of cytochrome p450 3a yields new mouse models for understanding xenobiotic metabolism. *J. Clin. Invest.* **117,** 3583–3592
56. Westlind, A., Malmebo, S., Johansson, I., Otter, C., Andersson, T. B., Ingelman-Sundberg, M., and Oscarson, M. (2001) Cloning and tissue distribution of a novel human cytochrome p450 of the CYP3A subfamily,

CYP3A43. *Biochem. Biophys. Res. Commun.* **281,** 1349–1355
57. Sakuma, T., Shimojima, T., Miwa, K., and Kamataki, T. (2004) Cloning CYP2D21 and CYP3A22 cDNAs from liver of miniature pigs. *Drug Metab. Dispos.* **32,** 376–378
58. Williams, P. A., Cosme, J., Vinkovic, D. M., Ward, A., Angove, H. C., Day, P. J., Vonrhein, C., Tickle, I. J., and Jhoti, H. (2004) Crystal structures of human cytochrome P450 3A4 bound to metyrapone and progesterone. *Science* **305,** 683–686
59. Nissen, P. H., Wintero, A. K., and Fredholm, M. (1998) Mapping of porcine genes belonging to two different cytochrome P450 subfamilies. *Anim. Genet.* **29,** 7–11
60. Johnsen, H., Odden, E., Lie, O., Johnsen, B. A., and Fonnum, F. (1986) Metabolism of T-2 toxin by rat liver carboxylesterase. *Biochem. Pharmacol.* **35,** 1469–1473
61. Hosokawa, M. (2008) Structure and catalytic properties of carboxylesterase isozymes involved in metabolic activation of prodrugs. *Molecules* **13,** 412–431
62. Wei, R. D., and Chu, F. S. (1985) Modification of *in vitro* metabolism of T-2 toxin by esterase inhibitors. *Appl. Environ. Microbiol.* **50,** 115–119
63. Young, J. C., Zhou, T., Yu, H., Zhu, H., and Gong, J. (2007) Degradation of trichothecene mycotoxins by chicken intestinal microbes. *Food Chem. Toxicol.* **45,** 136–143